TÉCNICO LISBOA

Impact of the Use of Beamforming Techniques in 5G Mobile Networks

Tiago Marques Santos

Thesis to obtain the Master of Science Degree in

Electrical and Computer Engineering

Supervisor: Prof. António José Castelo Branco Rodrigues

Examination Committee

Chairperson: Prof. José Eduardo Charters Ribeiro da Cunha Sanguino
Supervisor: Prof. António José Castelo Branco Rodrigues
Member of the Committee: Prof. Pedro Joaquim Amaro Sebastião
Eng. Augusto Silva

February 2021

Declaration

I declare that this document is an original work of my own authorship and that it fulfills all the requirements of the Code of Conduct and Good Practices of the Universidade de Lisboa.

Declaração

Declaro que o presente documento é um trabalho original da minha autoria e que cumpre todos os requisitos do Código de Conduta e Boas Práticas da Universidade de Lisboa.

Acknowledgments

I would like to start by thanking Prof. António Rodrigues for allowing me to be a part of this amazing project and welcoming me into the Radio Systems – Lisboa research group from Instituto de Telecomunicações. Also, some special thanks for the possibility of accomplishing this work in collaboration with Vodafone Portugal.

I want to express all my gratitude towards my mentor throughout this journey, Eng. Augusto Silva, who followed my work from Vodafone's point of view and helped me with his advice and support. Thank you for always being there to answer my questions, for all the guidance and encouraging words and for always believing in me. Thank you to each and everyone at Vodafone for being so welcoming and kind since day one. Special acknowledgments to Eng. António Fragoso and Eng. Rui Espadinha. This experience would not have been the same without all of them.

A huge thanks to all my friends and colleagues that accompanied me throughout during my time at Instituto Superior Técnico: Cátia, Daniel, Catarina, Luís, João, Francisco, Inês, Orlando, Andreia, Christopher, Miguel, Manuel, Jorge and André. Special thanks to all the incredible people that I worked with at NEECIST. You made my college life a different and better experience.

Thank you Beatriz, Pedro, Valter and Eduardo. You are all great people and I hope that the future rewards you for what you are.

Last, but not least, special thanks to my entire family. To my parents Maria do Carmo and Eduardo, for always believing that I would be able to overcome this stage. Thank you for the education you have provided and for always keeping me on the right path. To my brother André for always being an example to follow and for helping me when I needed it most. To my grandparents and uncles for the affection and pride with which they have always treated me. Nothing would have been possible without your support. Thank you.

Abstract

The objective of this dissertation is to study the impact that beamforming techniques have on a 5G mobile network, relative to the coverage of a base station. As 5G will be implemented based on a non-standalone topology, for the user to be able to use the network, he also needs 4G network coverage. Thus, it was intended to test the coverage limits between the 5G solution installed in the 3500 MHz band and the installed 4G solution, as well as to forecast the distribution of the beams and the transfer rate of the various users. A coverage simulator was implemented and coverage tests were carried out on the mobile network of the Vodafone operator in order to validate the results obtained. The basis of the simulator is the model developed in the METIS project that takes advantage of the calculation of losses along the path between the base station and the user's terminal.

Keywords

5G; Coverage; Beamforming; MIMO; Base stations.

Resumo

O objetivo desta dissertação é estudar o impacto que as técnicas de beamforming têm numa rede móvel 5G, relativamente à cobertura de uma estação base. Como o 5G será implementado com base numa topologia non-standalone, para que o utilizador consiga utilizar a rede, precisa também de cobertura de rede 4G. Assim, pretendeu-se testar os limites de cobertura entre a solução 5G instalada na banda 3500 MHz e a solução 4G instalada, bem como fazer uma previsão da distribuição dos beams e da taxa de transferência dos vários utilizadores. Foi implementado um simulador de cobertura e foram feitos testes de cobertura da rede móvel do operador Vodafone de forma a validar os resultados obtidos. A base do simulador é o modelo desenvolvido no projecto METIS que tira partido do cálculo das perdas ao longo do caminho entre a estação base e o terminal do utilizador.

Palavras Chave

5G; Cobertura; Beamforming; MIMO; Estações base.

Contents

List of Figures

List of Tables

Acronyms

1G 1st Generation

2G 2nd Generation

3D Three Dimensional

3G 3rd Generation

3GPP 3rd Generation Partnership Project

4G 4th Generation

5G 5th Generation

BS Base Station

CQI Channel Quality Indicator

EMBB Enhanced Mobile Broadband

FR1 Frequency Range 1

FWA Fixed Wireless Access

gNB next Generation Node B

IMT-2020 International Mobile Telecommunications-2020

IoT Internet of Things

ITU-R Radiocommunication Sector of the International Telecommunication Union

LoS Line of Sight

LTE Long Term Evolution

MCS Modulation and Coding Scheme

MIMO Multiple Input Multiple Output

MISO Multiple Input Single Output

MMTC Massice Machine Type Communications

MT Mobile Terminal

Non-LoS Non Line of Sight

NR New Radio

O2I Outdoor-to-Indoor

O2O Outdoor-to-Outdoor

PCI Physical Cell Identifier

PRB Physical Resource Block

QAM Quadrature Amplitude Modulation

QPSK Quadrature Phase Shift Keying

RAN Radio Access Network

SCS Sub-carrier Spacing

SIMO Single-input Multiple-output

SINR Signal to Interference Plus Noise Ratio

SISO Single-input Single-output/soft-input Soft-output

SMS Short Message Service

TDD Time Division Duplex

UE User Equipment

URLLC Ultra-reliable and Low Latency Communications

1

Introduction

Contents

1.1 Topic Overview

Over the last few years, quite a few changes have happened in mobile wireless communications, affecting people's daily lives and, above all, the economy and development of the various countries, all over the world. In general, they have been endlessly evolving to fulfil increasing demands and higher specification requirements.

A long time ago, in 1st Generation (1G), where analogue communications were used, it was only possible to make voice calls. After this, the digital communications appeared and, in 2nd Generation (2G), it became possible to send Short Message Service (SMS) and use mobile data with a low bit rate. With the 3rd Generation (3G) appeared the video calls and the experience surfing the internet was improved due to the increase of the binary flow. The need for multimedia services on mobile devices led to 4th Generation (4G) being developed, in which the bit rate was already much higher than that offered by previous generations.

With the great technological developments that have arisen in the area of multimedia contents, the increase in video consumption by end users has significantly increased. By 2018, 60% of the 27 EB total monthly traffic from mobile networks was due to video services, and in 2024, this number is expected to increase to 74% of the 136 EB total monthly traffic [1], as shown in Figure 1.1.

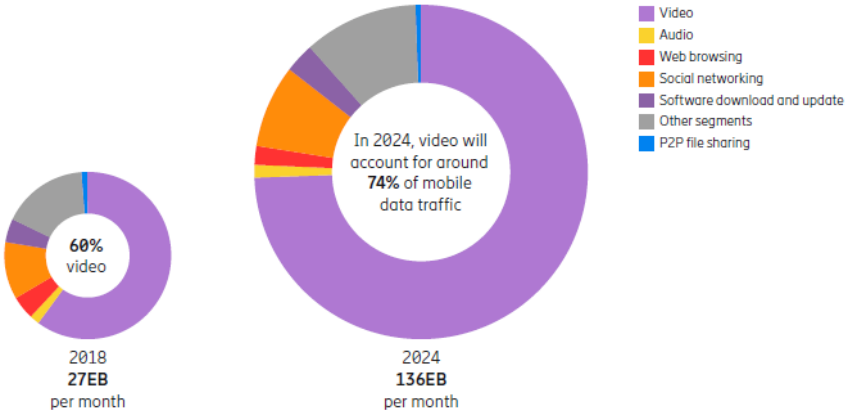

Figure 1.1: Mobile data traffic by application category per month between 2014 and 2024 (extracted from [1]).

Although video encoding become increasingly robust and efficient, with high-resolution video switching to 4K or even 8K resolutions, data volume continues to increase. Thus, it is clear that it is a growing challenge for today's networks support this huge amount of traffic on the network, resulting in the need to create a new standard for mobile networks, the 5th Generation (5G). According to Ericsson [1], the total mobile data traffic is predicted to be 5 times higher in 2024 than it was in 2018 and it is expected that 5G will carry 25 percent of mobile data traffic worldwide at that time. Thus, key drivers for 5G deployment should include the increase of network capacity and the decrease of cost per byte. The evolution of the global mobile data traffic is presented in Figure 1.2.

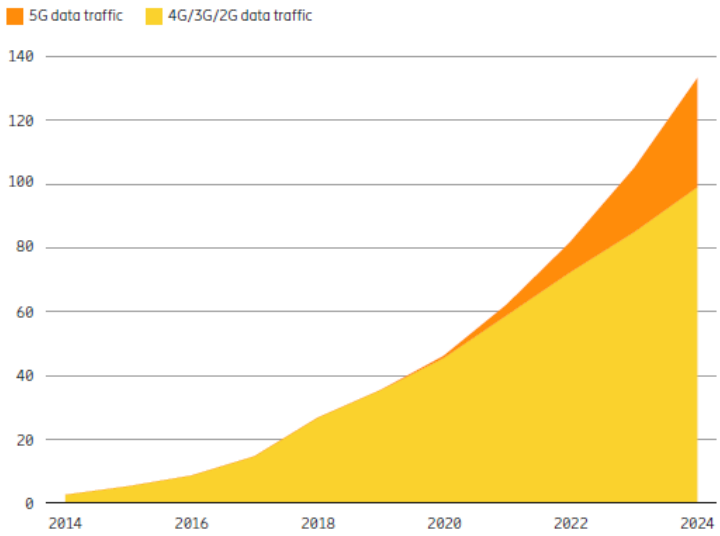

Figure 1.2: Area chart with the number of global mobile data traffic (EB per month), 2018-2014, (extracted from [1]).

On the other hand, the number of subscribers should increase as well. In 2018 there were approximately 8 billion enhanced mobile broadband globally subscribers and are expected 8.9 billion by the end of 2024, of which 1.5 billion (17 %) will be 5G subscriptions [1]. Currently, 4G is the dominant access technology. The amount of 4G subscriptions will still increase powerfully and is forecast to achieve 5.4 billion (60 percent) by the end of 2024. Finally, the amount of 2G and 3G subscriptions has declined over time and is predicted to continue with this trend till 2024, when 3G will have around 17 % of all mobile subscriptions and 2G can have a fair lower residual value. Figure 1.3 presents mobile subscriptions by technology, excluding Internet of Things (IoT) connections and Fixed Wireless Access (FWA) subscriptions.

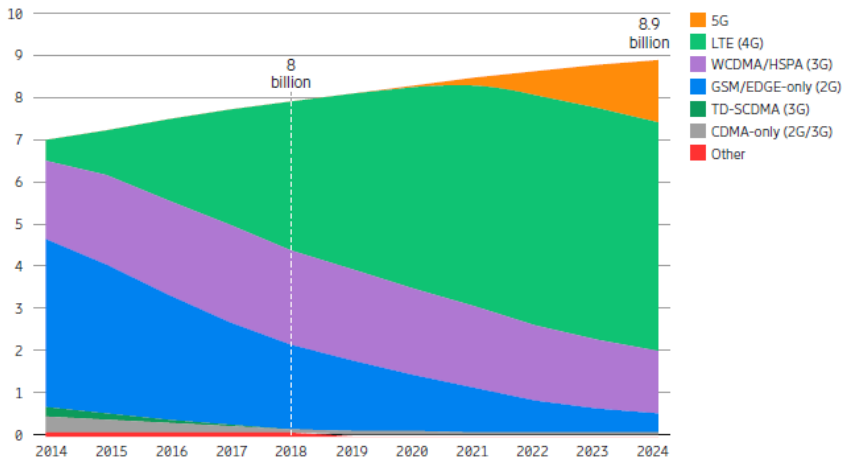

Figure 1.3: Area chart with the number of mobile subscriptions by technology (billion), 2018-2014, excluding IoT connections and FWA subscriptions (extracted from [1]).

Analysing Figure 1.3, the increase may seem quite significant, however the number of mobile subscriptions is greatly reduced when compared to IoT devices. As shown in Figure 1.4, this figure is expected to increase gradually as in 2018 there were about 8.6 billion IoT devices and by 2024 it is estimated that there 22.3 billion.

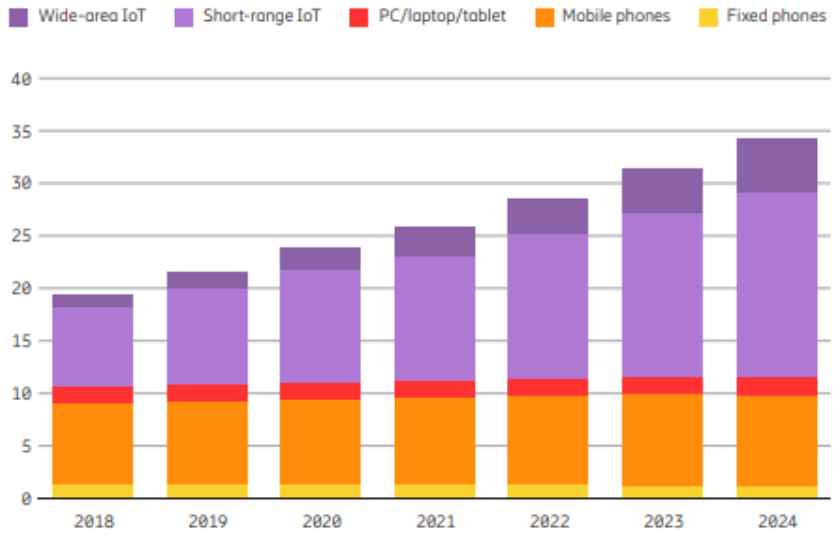

Figure 1.4: Area chart with the connected devices (billion), 2018-2014 (extracted from [1]).

Thus, another key 5G is precisely able to withstand the multitude of devices that are expected to exist in 2024, being the IoT ones fairly representative.

1.2 Motivation and Contents

Implementing a mobile network like 5G has a lot of challenges in its way, so it is important to take into account elements such as complexity of implementation, frequency bands, the modulation used, number of antennas in the Base Station (BS) and a Mobile Terminal (MT), etc.

This thesis was developed in collaboration with *Vodafone Portugal – Comunicações Pessoais, S.A.*, which belongs to *Vodafone Group Plc*, a multinational network operator. As a consequence of this partnership with an operator that tries to take advantage of the latest technological solutions in the market, this thesis came from a real-world problem. Since the 5G will initially be supported by a non-standalone technology, it is necessary that the mobile terminals have simultaneous coverage of 4G and 5G to take full advantage of the network.

The main purpose of this thesis is to make a comparison between a 5G New Radio implementation using the 3500 MHz frequency band and an LTE 1800 MHz network solution, mainly in terms of coverage. According to the classical models, being different frequencies, it is expected that the 3500 MHz solution has less reach than the 1800 MHz one. However, with the technological leap from a ”traditional”

technology to a beamforming one, doubts arise as to whether it is possible to achieve the same coverage area.

Hence, the predicted main output of this thesis is to confirm if it is possible to serve the same coverage area in various scenarios. Toward this aim, a simulator will be developed to validate the mentioned problem, depending on the variations of its various input parameters.

This document consists of 5 chapters, including this one.

Chapter 2 presents some fundamental concepts associated with 5G and is where a review of the state of the art is made.

Chapter 3 states the adopted methodologies and a brief description of the simulator.

Chapter 4 presents an analysis of the data taken from the simulator, as well as the data collected from the Vodafone Portugal live network.

Chapter 5 concludes this document with some conclusions and suggestions for future work.

2

Scientific Context and State of the Art

Contents

2.1 Services and Applications

This section is based on [2], [12], [13] and [14]. According to Radiocommunication Sector of the International Telecommunication Union (ITU-R), new services provided by 5G networks in International Mobile Telecommunications-2020 (IMT-2020) can be formalised in three important categories for IMT-2020: Enhanced Mobile Broadband (EMBB), Ultra-reliable and Low Latency Communications (URLLC) and Massice Machine Type Communications (MMTC), as shown in the Figure 2.1.

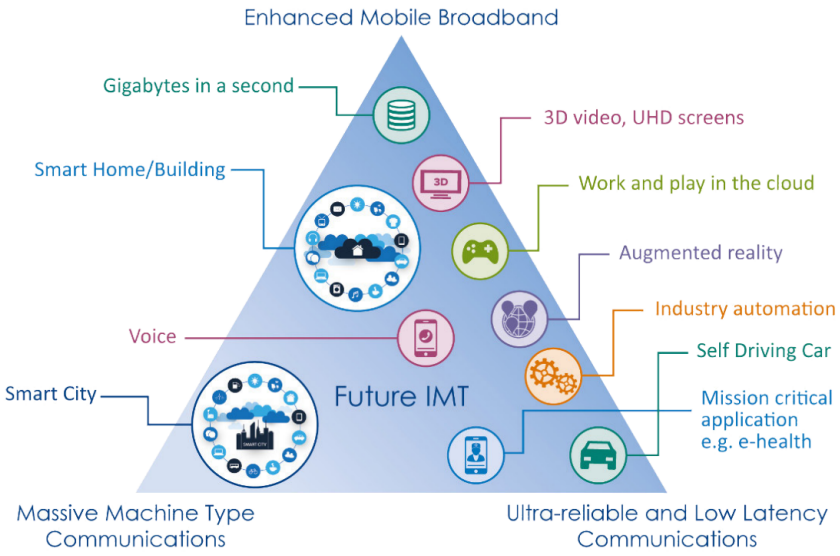

Figure 2.1: 5G usage scenarios (extracted from [2]).

EMBB addresses the ”human-centric” use cases, bringing high-speed mobile broadband to crowded areas, enabling consumers to enjoy high-speed streaming on demand and allowing enterprise collaboration services to evolve. It is also expected to be the primary use case for 5G in its early deployments and should include peak download speeds of at least 20 Gbps.

URLLC allows mission-critical applications, industrial automation, new medical applications, interactive games, augmented reality, communications to/from drones and autonomous vehicles. In this situation, any network latency or loss in signal coverage can have disastrous consequences. There should be sub-1ms latency and very high availability, reliability and security.

MMTC will allow you to support a huge amount of IoT devices (at least one million IoT connections per square kilometre) that usually transmit a relatively low volume of non-delay-sensitive data, with enhanced coverage and long battery life.

As suggested by Figure 2.1, these three categories encompass multiple day-to-day services and applications, all of them with slightly different requirements.

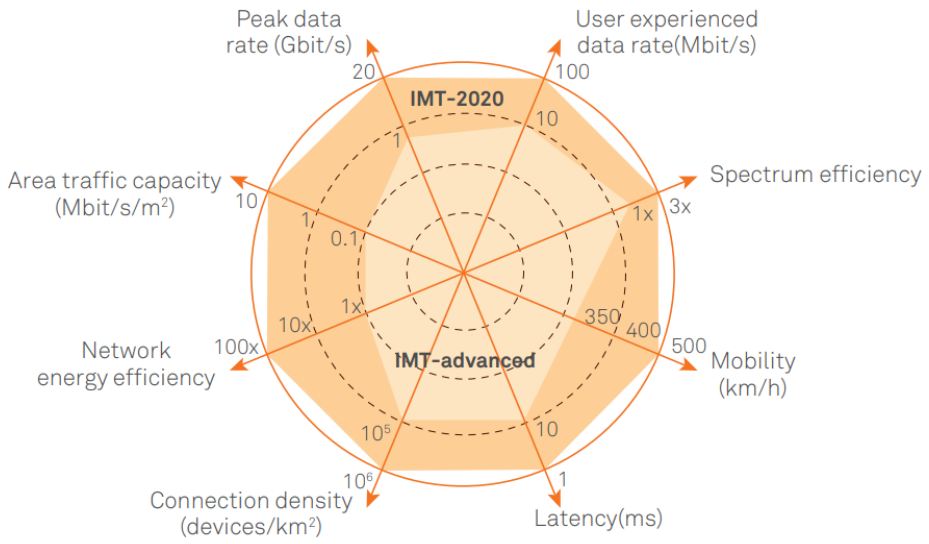

Figure 2.2: IMT-2020 usage scenarios and key capabilities extracted from [3]).

2.2 Radio Spectrum

Whenever a new generation of mobile communications appears, it is customary to allocate new radio spectrum. Usually, this happens by rearranging the spectrum of non-cellular applications (if this is allowed). Doing a retrospective of what happened in the past, it turns out that, for example, the fourth generation started focused at 800 MHz and the remaining bands were added later. As before, the same phenomenon will happen in 5G licensed spectrum but it is expected that 5G will also take advantage of the unlicensed spectrum. Figure 2.3 displays indicative spectrum allocation over time.

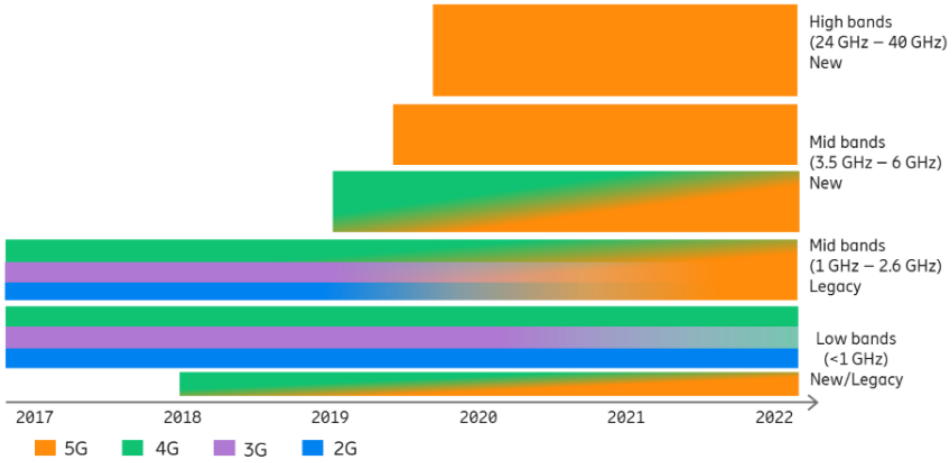

Figure 2.3: Indicative spectrum allocation over time (extracted from [4]).

In Europe, 5G will initially appear at 3.5 GHz band but it will be also present in low (below 1 GHz)

and high bands (above 24 GHz). Thus, according to [15] and [4], the 5G spectrum is divided into:

- A low band at 700 MHz: Mainly used for long range, widespread coverage communications and massive IoT.
- A mid-band at 3.5 GHz: This will likely be the key band for 5G, used for EMBB and compromise between coverage and capacity, although since it is at frequencies above those previously used for mobile, it could have some concerns to solve regarding the reduced range.
- A high band above 24 GHz: This might be used for very high throughput services for EMBB, localized deployments and low latency use cases, such as industrial IoT and venues, or for other applications that could require extreme bandwidth values, such as FWA.

In order to plan the future, some advances are beginning to emerge from equipment suppliers with the purpose of taking full advantage of technological developments. Ericsson, for example, proposes a stepwise smooth introduction to 5G using network patterns that use and combine current technologies and spectrum assets [4]. These proposed solutions include dual connectivity between 4G and 5G, spectrum sharing (4G / 5G carriers sharing the same spectrum) and inter-band carrier aggregation. Figure 2.4 displays an example of a stepwise introduction of 5G, the various frequency bands used and some possible performance characteristics in each step.

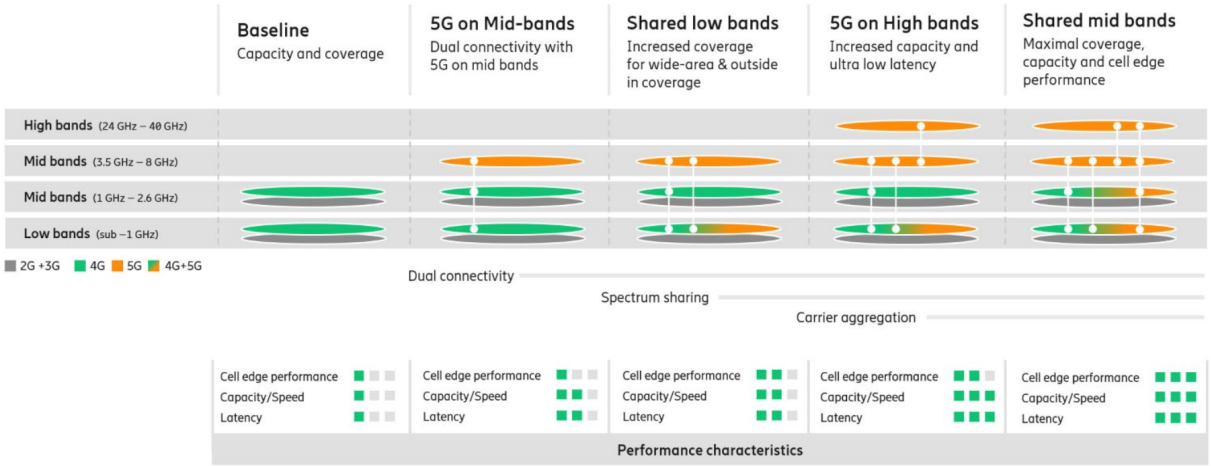

Figure 2.4: Example of a stepwise introduction of 5G (extracted from [4]).

According to [16], [9], [10] and [17] the New Radio (NR) operating bands are already defined by 3rd Generation Partnership Project (3GPP).

In frequency range 1, commonly known as above 6GHz, the available frequencies are presented in Table 2.1.

Regarding this, there are also some available bands for 5G in millimetre wave spectrum, as presented in Table 2.2

Table 2.1: NR operating bands in FR1 (adapted from [9]).

NR operating band	Uplink operating band BS receive / UE transmit	Downlink operating band BS transmit / UE receive	Duplex Mode
B1	1920 MHz – 1980 MHz	2110 MHz – 2170 MHz	FDD
B2	1850 MHz – 1910 MHz	1930 MHz – 1990 MHz	FDD
B3	1710 MHz – 1785 MHz	1805 MHz – 1880 MHz	FDD
B5	824 MHz – 849 MHz	869 MHz – 894 MHz	FDD
B7	2500 MHz – 2570 MHz	2620 MHz – 2690 MHz	FDD
B8	880 MHz – 915 MHz	925 MHz – 960 MHz	FDD
B12	699 MHz – 716 MHz	729 MHz – 746 MHz	FDD
B14	788 MHz – 798 MHz	758 MHz – 768 MHz	FDD
B18	815 MHz – 830 MHz	860 MHz – 875 MHz	FDD
B20	832 MHz – 862 MHz	791 MHz – 821 MHz	FDD
B25	1850 MHz – 1915 MHz	1930 MHz – 1995 MHz	FDD
B28	703 MHz – 748 MHz	758 MHz – 803 MHz	FDD
B30	2305 Mhz – 2315 MHz	2350 MHz – 2360 MHz	FDD
B34	2010 MHz – 2025 MHz	2010 MHz – 2025 MHz	TDD
B38	2570 MHz – 2620 MHz	2570 MHz – 2620 MHz	TDD
B39	1880 MHz – 1920 MHz	1880 MHz – 1920 MHz	TDD
B40	2300 MHz – 2400 MHz	2300 MHz – 2400 MHz	TDD
B41	2496 MHz – 2690 MHz	2496 MHz – 2690 MHz	TDD
B48	3550 MHz – 3700 MHz	3550 MHz – 3700 MHz	TDD
B50	1432 MHz – 1517 MHz	1432 MHz – 1517 MHz	TDD
B51	1427 MHz – 1432 MHz	1427 MHz – 1432 MHz	TDD
B65	1920 MHz – 2010 MHz	2110 MHz – 2200 MHz	FDD
B66	1710 MHz – 1780 MHz	2110 MHz – 2200 MHz	FDD
B70	1695 MHz – 1710 MHz	1995 MHz – 2020 MHz	FDD
B71	663 MHz – 698 MHz	617 MHz – 652 MHz	FDD
B74	1427 MHz – 1470 MHz	1475 MHz – 1518 MHz	FDD
B75	N/A	1432 MHz – 1517 MHz	SDL
B76	N/A	1427 MHz – 1432 MHz	SDL
B77	3300 MHz – 4200 MHz	3300 MHz – 4200 MHz	TDD
B78	3300 MHz – 3800 MHz	3300 MHz – 3800 MHz	TDD
B79	4400 MHz – 5000 MHz	4400 MHz – 5000 MHz	TDD
B80	1710 MHz – 1785 MHz	N/A	SUL
B81	880 MHz – 915 MHz	N/A	SUL
B82	832 MHz – 862 MHz	N/A	SUL
B83	703 MHz – 748 MHz	N/A	SUL
B84	1920 MHz – 1980 MHz	N/A	SUL
B86	1710 MHz – 1780 MHz	N/A	SUL
B90	2496 MHz – 2690 MHz	2496 MHz – 2690 MHz	TDD

Table 2.2: NR operating bands in FR2 (adapted from [10]).

NR operating band	Uplink operating band BS receive / UE transmit	Downlink operating band BS transmit / UE receive	Duplex Mode
B257	26500 MHz – 29500 MHz	26500 MHz – 29500 MHz	TDD
B258	24250 MHz – 27500 MHz	24250 MHz – 27500 MHz	TDD
B260	37000 MHz – 40000 MHz	37000 MHz – 40000 MHz	TDD
B261	27500 MHz – 28350 MHz	27500 MHz – 28350 MHz	TDD

2.3 Radio Interface

2.3.1 MIMO

Multiple Input Multiple Output (MIMO) is a type of antenna that takes advantage of a set of receivers and transmitters to increase the efficiency of a transmission channel. Using multiple antennas configurations, shown in Figure 2.5, it is possible to take advantage of spatial multiplexing and spatial diversity.

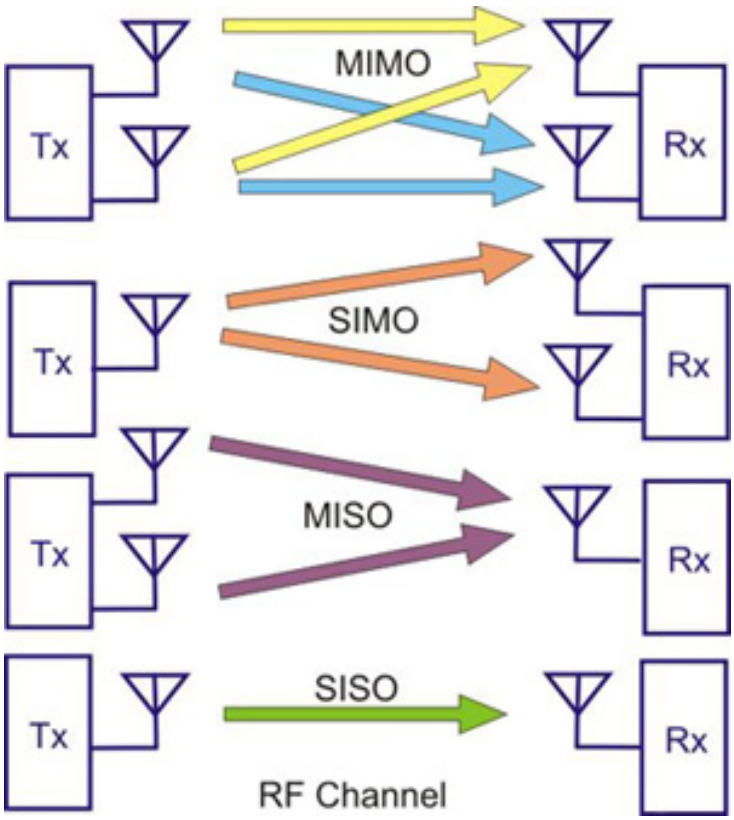

Figure 2.5: MIMO antenna configuration (extracted from [5]).

In the first situation in the Figure 2.5, with MIMO, it is possible to use spatial multiplexing in order to encode and send distinct signals (where the information is divided by the two signals on the transmitter side), leading to an increase of the transmitted information and, consequently, to an increase in the throughput. Since the transmission medium is the same and as there will be crossed terms, it is possible to use dispersing matrix H to obtain the cross terms on the receiver side.

In the second and third situations in Figure 2.5, corresponding to Single-input Multiple-output (SIMO) and Multiple Input Single Output (MISO), spatial diversity is used, allowing multiple ”copies” of the same signal to be received at the receiver or sent to the transmitter, respectively. This increases the probability of the signal reaching the destination.

Lastly, the fourth situation in Figure 2.5, a classic Single-input Single-output/soft-input Soft-output

(SISO) configuration is used in which one can not take advantage of the aforementioned gains.

The 5G systems are going to employ these techniques in a massive way, using the so-called Massive MIMO, Figure 2.6.

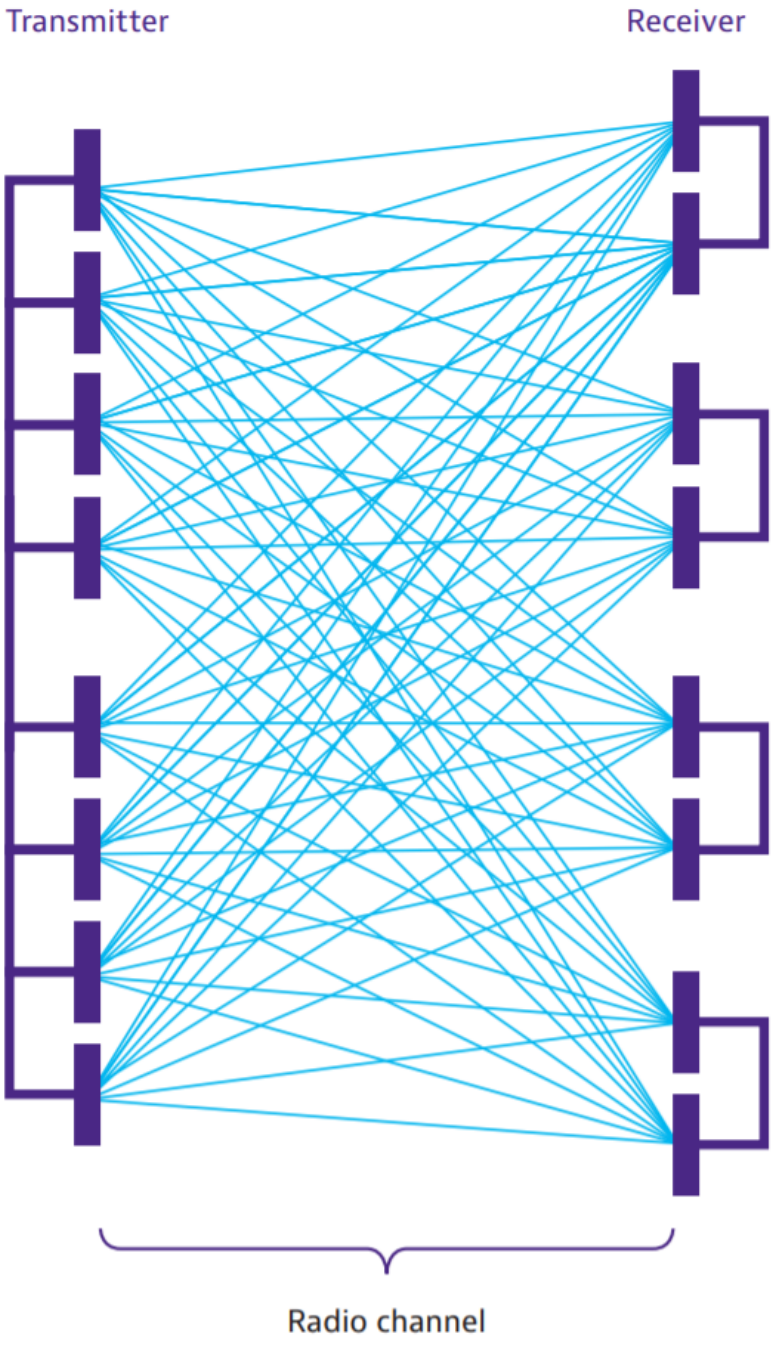

Figure 2.6: Radio channel in a Massive MIMO scheme

2.3.2 Beamforming

Beamforming is a signal processing technique that allows to direct radio energy through the radio channel toward a specific receiver, that is, to orient the various beams of an antenna, and consequently the radiation pattern, as required. In this way, by feeding separately each element of this matrix with different weights in both the horizontal and vertical domains, each beam can be directed in a certain direction. When the phase and amplitude of the transmitted signals is adjusted, constructive addition of the corresponding signals at the UE receiver can be achieved, which increases the received signal strength and thus the end-user throughput. On the other hand, beamforming also allows to collect the signal energy from a specific transmitter when receiving. So, both uplink and downlink can take advantage of these features. Just as an example, in Figure 2.7 is presented the system architecture of a 4 $\times$ 4 multibeam antenna.

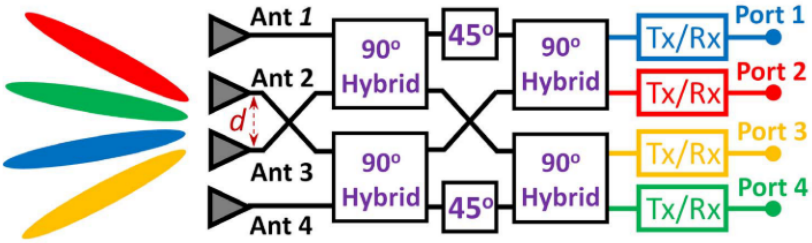

Figure 2.7: System architecture of a 4 $\times$ 4 multibeam antenna (extracted from [6])

Scaling the situation of the Figure 2.7 to a weighted phased array, spatial processing is allowed to be used in Three Dimensional (3D). By controlling the transmission radiation pattern in both the horizontal and vertical planes, the interference can be compressed or avoided, leading to improvements in spectrum efficiency and interference mitigation in cellular mobile communications. By using this technique there is still the advantage that could be not necessary to change the antenna array size of the base station and the antenna number of the terminal.

There are several possible classifications for the various types of beamforming however, one of the possible classifications indicated in [18] is based on signal processing. Presented by Hur et al. (2013) and Bogale and Le (2014), these techniques were classified as:

- Analogue Beamforming - very simple phase shifters but have the advantage of being cheaper compared to digital beamforming. Adopted in Massive MIMO systems.
- Digital Beamforming - are more accurate and rapid foundation results to obtain user signals but suffers from high complexity and an expensive design. Not adopted in Massive MIMO systems.
- Hybrid analogue/digital Beamforming - has been developed for massive MIMO systems to obtain some of the advantages of analogue and digital beamforming.

If users are well spatially distributed, there are even more significant gain improvements that are achieved since there is less interference between them. Figure 2.8 is an illustration of 3D-MIMO using beamforming.

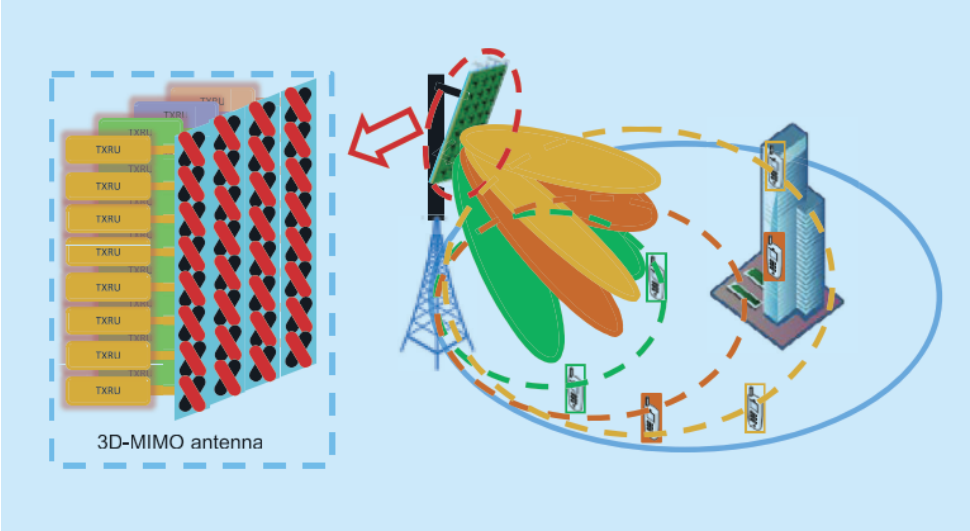

Figure 2.8: Illustration of 3D-MIMO (extracted from [7])

According to [19], in order to manage beamforming there are a number of important procedures that are performed:

- Beam sweeping - covering a spatial area with a set of beams transmitted and received according to pre-specified intervals and directions.
- Beam measurement - the evaluation of the received signal at the gNB or at the UE. This can be made by using several metrics such as Signal to Interference Plus Noise Ratio (SINR) or the received power.
- Beam determination - the selection of the suitable beam or beams either at the base station or at the User Equipment (UE), according to the measurements obtained with the beam measurement procedure.
- Beam reporting - procedure used by the UE to send beam quality and beam decision information to the Radio Access Network.

In order to estimate coverage it is necessary to consider several parameters, such as test scenario, frequency used and bandwidth allocated. Thus, to have an idea of the covered range it is necessary to use SINR at the receiver side to obtain the acceptable path loss. Using a propagation model that fits in the study case scenario, it is possible to obtain the maximum range where the quality parameters are acceptable and even a throughput approximation.

2.4 State of the art

In this section, a short approach is taken to the study developed in the research area of the dissertation problem. In each project is presented a brief description of the scenario, the methods used, results obtained and/or some conclusions.

D. Kurita et al. [20] performed an outdoor 5G trial in the Tokyo Odaiba, Japan, using the 28-GHz frequency band. The base stations were installed in buildings, in a waterfront area, and allowed researchers to evaluate some technologies such as MIMO antennas (either the base station or the mobile terminal), beamforming and beam tracking, use of the high 28-GHz frequency, the wide frequency bandwidth of 400 MHz and a coverage area in a realistic urban deployment. This study revealed that it was possible to achieve throughputs exceeding 1 Gbps in the experiment area and approximately 200 Mbps at 500 m away from the BS. On the other hand, it was also confirmed that beam tracking and baseband unit handover together ensured that high path loss in the 28-GHz band was balanced to achieve a coverage area of 500 m. Lastly, by using the above frequency range, the Line of Sight (LoS) and Non Line of Sight (Non-LoS) conditions were critical to 5G performance and could lead to a drop in the connection when there is an obstacle between the MT and a BS.

A group of researchers from Ghent University, Belgium [21], analysed the impact of using beamforming on the design of an energy efficient 5G mobile network (at 60 GHz with a 500 MHz bandwidth). A realistic suburban area of 6.85 km^2, in Ghent, was used for the simulations in which the network should support 224 simultaneous active users and at least 95% users were served. This study yielded the following results: the 5G network scenario without beamforming implemented required more base stations than the 4G reference scenario (at 2.6 GHz with a 20 MHz bandwidth) but it was 50% less power consumed and provided 2 times more capacity than 4G; the 5G network scenario with beamforming implemented was 3-4 times more energy efficient than 4G reference scenario and network coverage performed similarly to the 4G.

According to China Mobile Research Institute [7], China Mobile and some partners started its 5G NR trials in the university city of Guangzhou since 2015. These trials had a typical dense urban scenario and aimed to understand the fundamental performance of the 5G NR air interface (especially for EMBB and URLLC scenarios), to validate the hardware architecture of the 3D-MIMO (using an antenna with 192 elements) and which was the potential early market of 5G. Based on a typical cell throughput of 40 Mbps / 20 MHz for Long Term Evolution (LTE) Time Division Duplex (TDD) system 20-fold throughput gain could be achieved by 3D-MIMO and, that way, it was expected that 5G spectrum efficiency would be 3-5 times improved compared to 4G. Thus, the main result of this study was the fact that goals of the 5G system design, like 2 Gbps data rate, 20-fold improvement in cell throughput compared with that of 4G and 1 ms latency of the air interface were achievable.

3

Model and Simulator Description

Contents

3.1 Scenario Characterisation

The model developed in this thesis aims to create a 5G mobile network coverage and capacity simulator in the surroundings of Vodafone Portugal's headquarters building in Parque das Nações, in Lisbon. Figures 3.1 and 3.2 are an aerial and a top view of Vodafone's headquarters surroundings, respectively.

Figure 3.1: Aerial view of Vodafone's headquarters surroundings

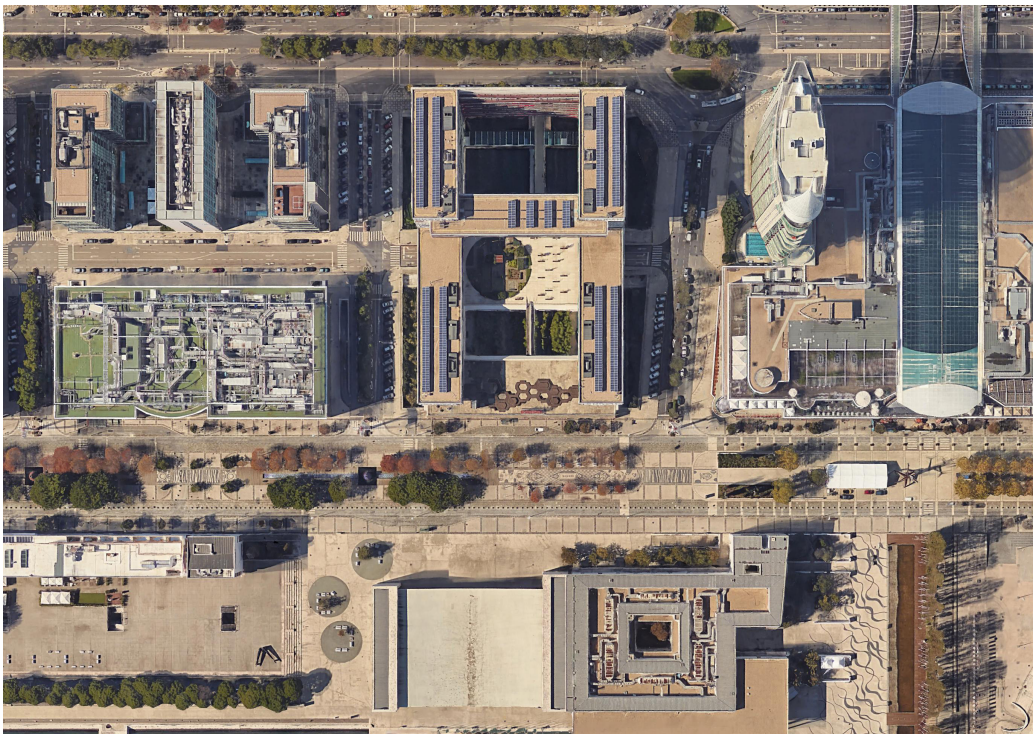

Figure 3.2: Top view of Vodafone's headquarters surroundings

Given that next Generation Node B (gNB) have quite distinct particularities and characteristics compared to the models of base stations of previous generations, it is important to mention some characteristics of the antenna model and the surrounding scenario.

First of all, there is a need to define the type of scenario and connectivity environment. The surroundings of the Vodafone building are an area of the city mainly made up of buildings, but there are relatively wide areas of open space with a direct viewing angle for the antenna given the position of the antennas(s). In the streets, there is also some vegetation, but generally dense and low in height. Thus, it is possible to classify the area around Vodafone Portugal as urban.

Since there are UEs both in outdoor and indoor environments, the communication environment is considered as Outdoor-to-Outdoor (O2O) and also Outdoor-to-Indoor (O2I), since the antennas are located on the rooftop of the Vodafone's building and the UEs can be distributed inside and outside the surrounding buildings.

The schematic of the scenario environment that will be used in the simulator is presented in figures 3.3 and 3.4. In the right corner of both figures, there is a bar where is possible to check the number of floors of each building.

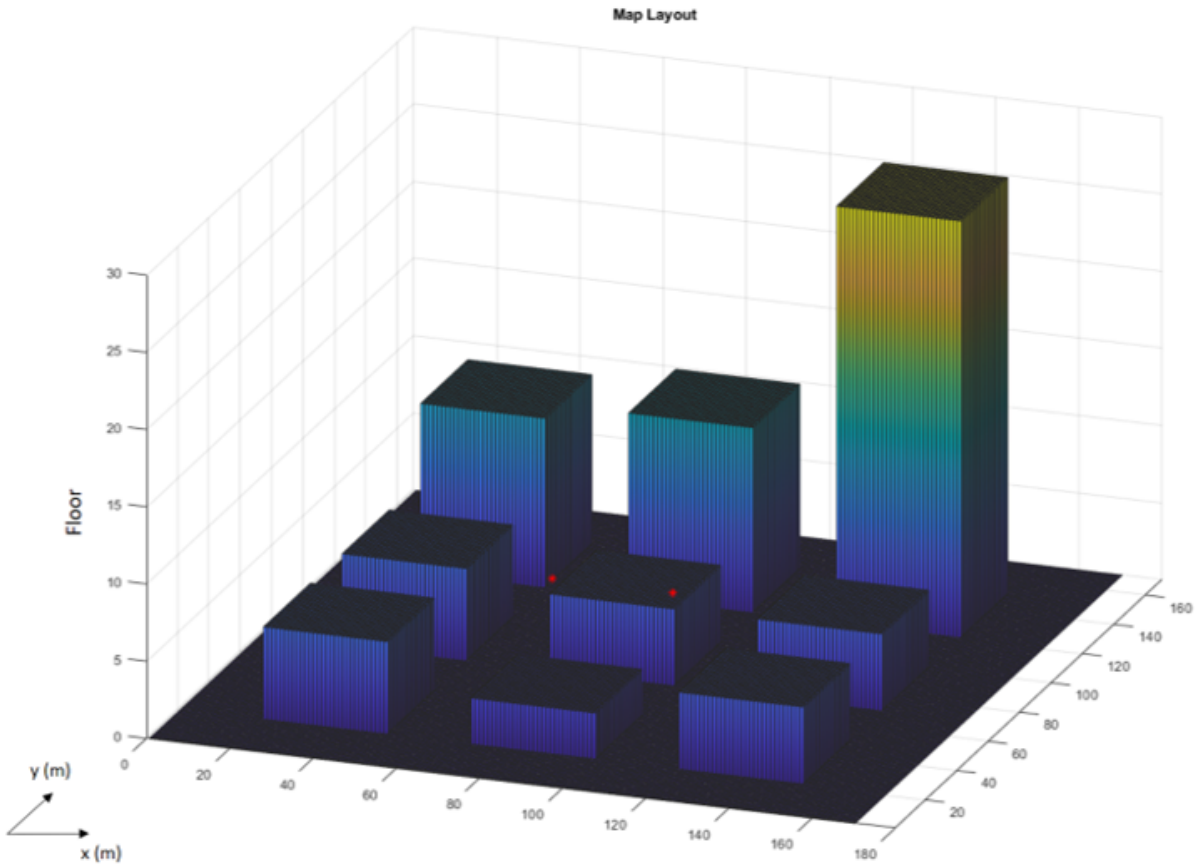

Figure 3.3: Aerial view of simulator's recreation of Vodafone's headquarters surroundings.

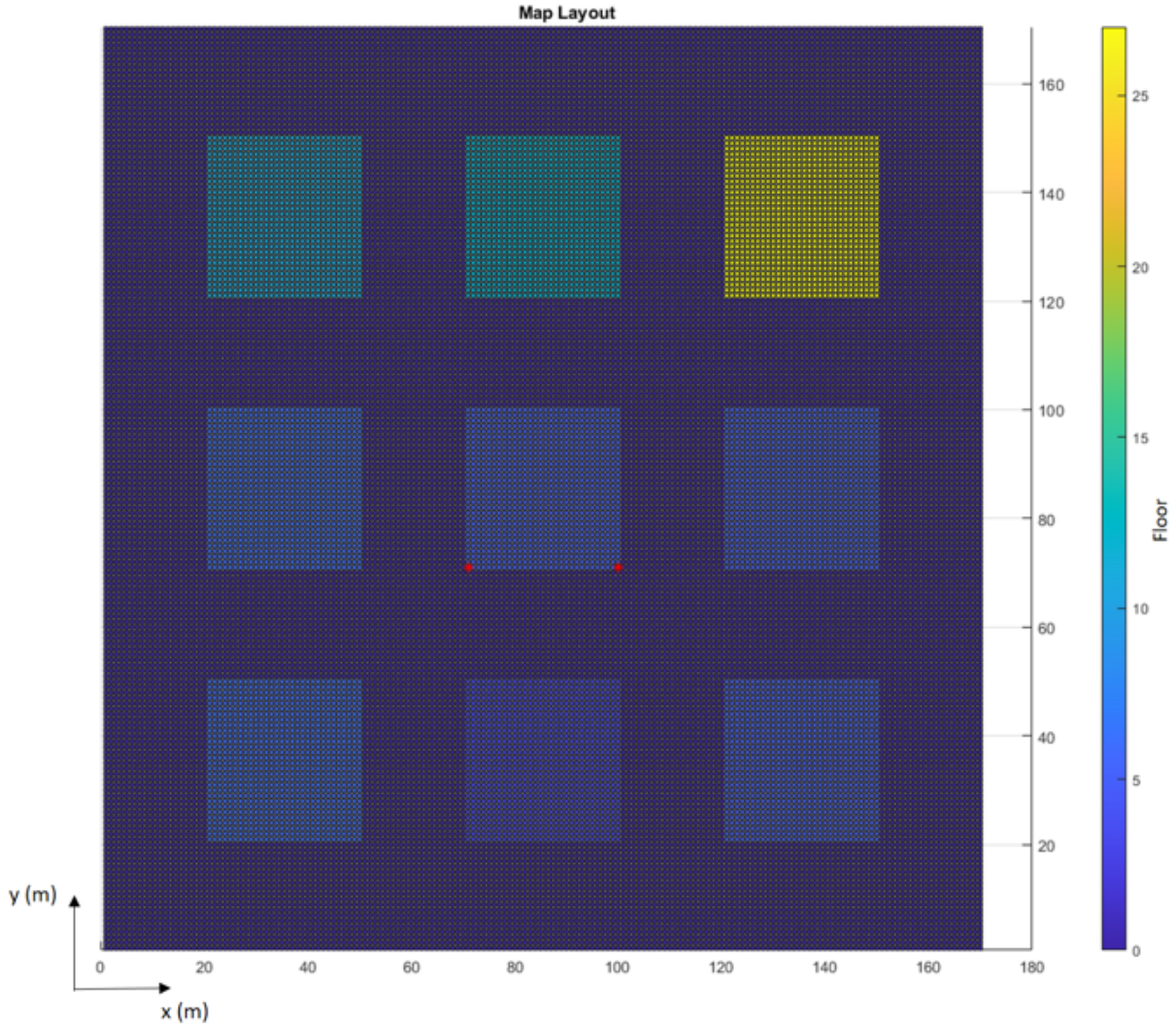

Figure 3.4: Top view of simulator's recreation of Vodafone's headquarters surroundings.

3.2 Antenna Specifications

The live network that is currently being used for tests in this area is composed of two 5G base stations, one in the left of the Vodafone building and another in the right, both at the riverside. These locations are marked in the figure 3.4.

The antenna model mounted in the area, in both base stations, takes advantage of advanced state-of-the-art techniques, namely massive MIMO and beamforming, capable to fully utilize radio resources in both azimuth and elevation. Compared to previous macro solutions, the key advantages are changes in: enhanced coverage (high gain adaptive beamforming), enhanced capacity (high-order spatial multiplexing and multi-user MIMO), advanced Radio Access Network (RAN) features (vertical and horizontal beamforming) and improved network performance (low inter-cell interference).

The antenna model that was chosen by Vodafone for this installation can be deployed in three distinct variations: Macro, Hotspot and Highrise. Each of these variations is adapted to a specific scenario. Table 3.1 provides the vertical and horizontal radiation beamwidths for broadcast beams each setup of the antenna, since each of these variations has different radiation patterns.

	Vertical Beamwidth (°)	Horizontal Beamwidth (°)
Macro	10	65
Hotspot	30	65
Highrise	30	20

Table 3.1: Radiation beamwidths for broadcast beams in each possible antenna setup.

As a consequence of these different beamwidth for broadcast beams, it is easy to understand that there are different number of traffic beams in each variation. Regarding traffic beams, it was not possible to obtain beamwidth of the beams in all directions. Through the manufacturer's specifications, presented in the datasheet, it was only possible to obtain these values for 3 directions. Table 3.2 provides the vertical and horizontal radiation beamwidths for traffic beams in the 3 mentioned directions.

Htilt(°), Vtilt(°)	Vertical Beamwidth (°)	Horizontal Beamwidth (°)
0, 3	9.5	12
5, 3	9.5	22
0, 18	10	12

Table 3.2: Radiation beamwidths for traffic beams in the 3 mentioned directions.

As the the information presented in Table 3.2 and this information is quite limited, turns out that it would not be enough to carry out the intended study. So, to overcome the problem of lack of information, the traffic beams of scenario setup was obtained not only from the manufacturer vertical and horizontal radiation beamwidths specifications and the .msi files itself. Thus, a traffic beam was defined whenever the tested gain was inside of the vertical and horizontal radiation beamwidths intervals, stated by the manufacturer.

Thus, each possible antenna setup has a different number of traffic beams and, depending on the UE distribution, is preferably recommended for a particular scenario.

From Table 3.1 and Table 3.2, it is easy to understand that:

- If the expected that if the majority of the users are, for example, in a urban scenario with high density buildings (most of the users probably in an indoor environment such as offices and tall residential buildings), it is expected that the chosen setup maximises the number of beams in the vertical plane, that is, Highrise. This solution provides a total of 30 beams.

- If users are placed in a horizontal plane, where there are few (or none) variations of user locations in the vertical plane, it is expected that the setup is chosen according to it. Thus, in this situation

the best solution would be a Macro setup since it has a higher horizontal weight compared to the vertical one. This is the typical scenario in a mobile network and this solution provides a total of 26 beams.

- Between the previous solutions, there is also the Hotspot solution that have the vertical beamwidth of Highrise and the horizontal beamwidth of Macro. This solution would be the smart choice for a scenario with high density of users, such as a special event, where there can be users in a wide area and in various directions. This is the solution that provides the higher number of beams, that is, a total of 78 beams.

Table 3.3 summarises this informations, presenting the number of traffic beams and the best use scenario for each possible antenna setup.

	Macro	Hotspot	Highrise
Number of Beams	26	78	30
Best Use Scenario	Horizontal Plane	Horizontal and Vertical Plane	Vertical Plane

Table 3.3: Number of Beams for each possible antenna setup.

To study the coverage of this 5G NR BS antenna model in the simulator and compare it with the real antenna model mounted in the area, although the simulator supports the 3 possible configurations, the analysis is intended to focus on evaluating the macro setup. This choice was made since that it is the one that usually best fits a usual scenario on the network and that, in this case, is what is configured on the spot. Moreover, as the frequency band used by Vodafone Portugal operator is around 3.6 GHz, in their live test network, the study done in this dissertation focuses on the frequency of 3.6 GHz, which is included in the Frequency Range 1 (FR1).

3.3 Simulator Description

In order to develop a simulator that can predict the expected coverage of a 5G mobile network in each point of a map, there are some aspects that needed to be taken into account.

This section provides general information on all the parameters to be set in the simulator, all the specifications, hypothetical conditions, and the planned simulation progress. The simulator has some versatility to run it in the tested scenario and/or in a similar one, i.e. it has different degrees of freedom to adapt the virtual simulator scenario with a certain reliability to a realistic one.

This simulator, created in Matlab, use outputs from METIS project [22] and from the previous work done by António Fragoso in his master thesis about ”Impact of Massive MIMO antennas on high capacity 5G-NR Networks” [8], also in partnership with Vodafone Portugal. This path was chosen because it is a simulator based on a map, which supports a frequency range up to 100 GHz, a bandwidth up to 10%

of the central frequency and allows support for antennas capable of taking advantage of Massive MIMO and beamforming. Although the METIS-based model supports 3D elevation using simplified ray tracing, another approach was initially attempted with true ray-tracing and a real map of the area involved, which would bring more precision and reliability compared to the METIS-based model, however, due to the strong computing requirements that the model was requiring, it made this approach unfeasible.

As in the mentioned studies, in this thesis it is assumed that UE can be in LoS or in Non-LoS. On the other hand, given the location where the UE is located, it can also be in an indoor or outdoor environment.

To have an accurate representation of the characteristics of the signal received at the position in each UE on the map, several parameters are taken into account to calculate the path loss between the base stations and the UE location.

3.3.1 Path Loss

In order to simplify the approach to the calculation of the path losses, consider only a base station, that is, the serving base station, and a UE. Later, this case will be generalised to the real environment of an operator, with the possibility of having several base stations and several UEs, such as the case studied.

As described above, UEs may be in an LoS or Non-LoS situation. Starting from the simplest case, in which there is LoS between the base station and the UE, without any object between them, it is possible to use the free space equation, presented in equation 3.1, to calculate the path loss, L_{fs}.

$$L_{fs} = -20 \log_{10} \left(\frac{\lambda}{4\pi R} \right) [dB] \tag{3.1}$$

being:

- λ: the wavelength;
- R: the 2D distance between the UE and the BS.

As the previous situation, without obstacles, covers a small number of UEs, it is necessary to take into account other parameters in case there is at least one relevant obstacle between it and the base station.

According to the aforementioned, there is a need to use the formula of equation 3.2, which, again, depends on the location of the terminal. This equation takes into account 2 new parameters: the attenuation caused by the diffraction on the walls of buildings, L_{msd}, and the one from the rooftop of buildings down to the street level, L_{rts}.

$$L_{out} = L_{fs} + L_{msd} + L_{rts} \tag{3.2}$$

Considering that the main obstacles that may exist are buildings, it is possible to make a representation of the path between the base station and the terminal and some important parameters, as shown in the figure 3.5.

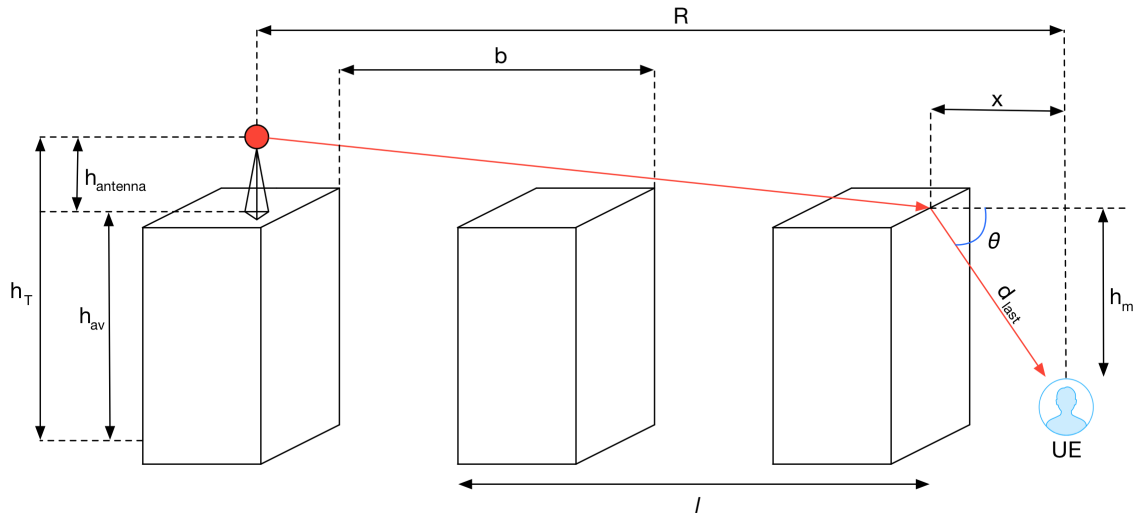

Figure 3.5: Representation of the path between the serving base station and the obstructed terminal at the street level (extracted from [8])

.

In case of multiple screen diffraction loss, from this figure it is possible to extract some information to calculate some types of losses depending on whether or not there are obstacles between the base station and the UE. As refered in [8], if the sum of all the path lengths covered by the intersection on buildings and streets l is larger than the settled field distance, d_s, the multiple screen diffraction loss is determined using the equation 3.3.

$$L_{msd} = L_{BSh} + k_a + k_d \times \log_{10}\left(R_{[km]}\right) + k_f \times \log_{10}\left(f_{[MHz]}\right) - 9\log_{10}\left(b\right)[dB] \tag{3.3}$$

being:

- d_s: parameter that indicates how loss of multiple screen diffraction is accomplished and it is measured as:

$$d_s = \frac{\lambda R^2}{h_{antenna}^2}[m] \tag{3.4}$$

- L_{BSh}: the loss that is correlated to the base station's height. It is null when the average rooftop's height h_{av} is above or at the same height of the antenna's. Otherwise, it can be expressed by:

$$L_{BSh} = -18\log_{10}\left(1 + h_{antenna}\right)[dB] \tag{3.5}$$

- k_a: parameter associated with the relationship between the height of the base station and what barriers are around it. According to propagation conditions, ka can have a total different value and is expressed by:

$$k_a = \begin{cases} 54, & for\ h_T > h_{av}; \\ 54 - 0.8\ h_{antenna}, & for\ h_T \leq h_{av}\ and\ R \geq 500m; \\ 54 - 1.6\ h_{antenna} R_{[km]}, & for\ h_T \geq h_{av}\ and\ R < 500m. \end{cases} \tag{3.6}$$

- k_d: parameter associated with the relationship between the height of the base station and what barriers are around it, such as k_a. According to propagation conditions, k_d is expressed by:

$$k_d = \begin{cases} 18, & for\ h_T > h_{av}; \\ 18 - 15\frac{h_{antenna}}{h_{av}} & for\ h_T \leq h_{av}. \end{cases} \tag{3.7}$$

- k_f: the impact of tree density on propagation, based on the surrounding environment scenario and expressed by:

$$k_f = \begin{cases} 0.7\left(\frac{f_{[MHz]}}{925} - 1\right) & for\ medium\ size\ cities\ and\ suburban\ centers; \\ 15\left(\frac{f_{[MHz]}}{925} - 1\right) & for\ metropolitan\ centers. \end{cases} \tag{3.8}$$

- b: the average value of all intersections covered by the ray's path on streets and buildings.

If the sum of all lengths covered by the ray's path on streets and buildings, l, is not larger than d_s, the height of rooftops and BS, Q_m have different values:

$$L_{msd} = -10 \log_{10} \left(Q_m^2\right)[dB] \tag{3.9}$$

being:

$$Q_m = \begin{cases} 2.35\left(\frac{h_{antenna}}{R}\sqrt{\frac{b}{\lambda}}\right)^{0.9} & for\ h_{antenna} > h_{av}; \\ \frac{b}{R} & for\ h_{antenna} \approx h_{av}; \\ \frac{b}{2\pi R}\sqrt{\frac{\lambda}{\sqrt{h_{antenna}^2 + b^2}}}\left(\frac{1}{\vartheta} - \frac{1}{2\pi + \vartheta}\right) & for\ h_{antenna} < h_{av}; \end{cases} \tag{3.10}$$

and:

$$\vartheta = \tan^{-1}\left(\frac{h_{antenna}}{b}\right) \tag{3.11}$$

In order to obtain the diffraction from the rooftop down to the street level, L_{rts}, it is important to differentiate the LoS from the Non-LoS environment:

$$L_{rts} = \begin{cases} -20\log_{10}\left(\frac{1}{2} - \frac{1}{\pi}\arctan\left((\theta)\sqrt{\frac{\pi^3}{4\lambda} \times d_{last} \times \left(1-\cos\theta\right)}\right)\right)[dB] & for Non-LoS; \\ 0 & for LoS; \end{cases} \tag{3.12}$$

being:

- d_{last}: the distance between the user and the diffraction point on the rooftop of the building nearest to the UE;
- θ: angle between the building standing closer to the user and the the ray.

Regarding the calculation of the losses associated with the users located in the interior of the buildings, when a UE is in this situation it will inevitably have an additional loss due to the penetration in the walls of the building. In order to obtain this value, it is used the pah loss of the nearest outdoor point of each wall of the floor in which UE is located, $Loutdoors$. Thus, it is important to compute all the values relevant to any outdoor location beforehand in order to obtain the indoor values.

Being in an indoor position it is necessary to take into account the distance between the user and the walls:

$$L_{indoors} = \frac{1}{2}\, d_{each\ wall} \tag{3.13}$$

As the path between the base station and the terminal can be done directly or indirectly, that is, with a direct incident ray or the ray comes from one or multiple reflections. In this last case, with an indirect incident ray, METIS states that when the ray reflected by a building, when it passes between two buildings or when neighbour building is smaller than the receiver's point in space, then it is assumed that L_{th} is equal to 1000 dB, in order to perform a mathematical simplification. When the incident ray is direct L_{th} is obtained by:

$$L_{th} = 9.82 + 5.98\ \log_{10}\left(f_{[GHz]}\right) + 15\left(1-\sin\theta\right)^2[dB] \tag{3.14}$$

Thus, the total indoor loss is obtained by adding these parameters:

$$L_{ind} = L_{outdoors} + L_{th} + L_{indoors} \tag{3.15}$$

In general, in order to show the simulator's operation in calculating the path losses of all points on the map, the figure 3.6 presents the value of the losses for each point on the map, at ground level. It appears that the farther the user is from the serving cell, the higher the path loss value and that in an indoor environment the expected increase in the same parameter is also observed.

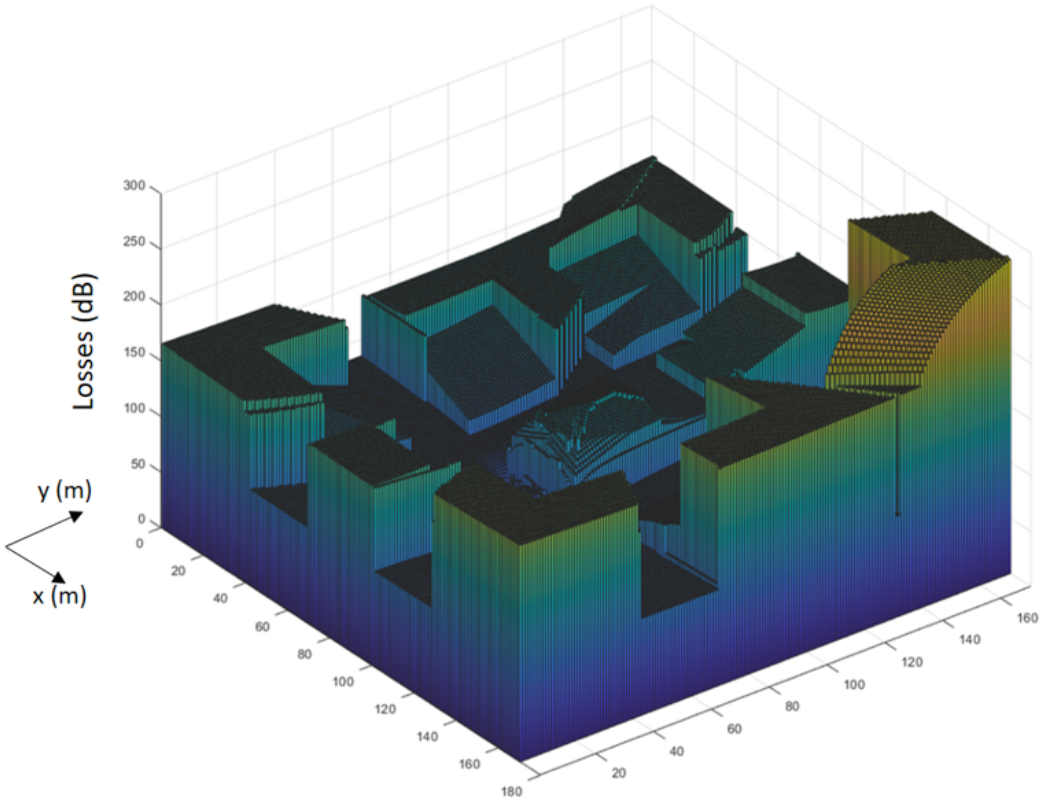

Figure 3.6: Path loss at the ground floor.

3.3.2 Which Base Station is Serving Cell?

The simulator scenario contains 2 base stations, previously shown in figure 3.4, namely base station 1 (on the left) and base station 2 (on the right).

To make the choice of the base station that serves each UE, it is necessary to perform some calculations. After calculating the path loss value between each base station and each UE location, this value is used to obtain the received power that arrives at each of these locations, according to 3.16.

$$P_{RX} = P_{TX} + Gains - Losses[dBm] \tag{3.16}$$

being:

- P_{RX}: the receiver power;
- P_{TX}: total radiated power on the antenna side;
- $Gains$: sum of horizontal beam gain, vertical beam gain and terminal's gain;
- $loss$: the path loss attenuation calculated for the UE location.

Figure 3.7 presents the power received in each location of the map at the ground floor.

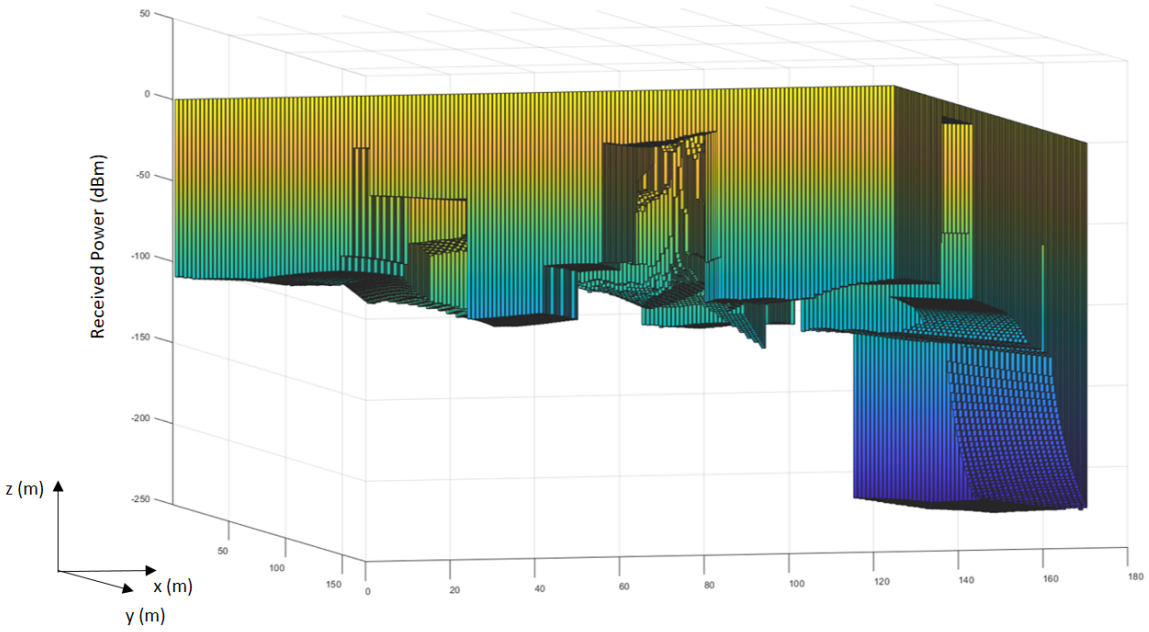

Figure 3.7: Received power in each location of the map, at the ground floor.

As can be seen, inside buildings there is a lower receiver power than in an outdoor environment, which would be expected due to indoor losses. It is also noted that the further away the base is located from the UE, the greater the value of losses and, consequently, the lower the value of received power. Thus, to obtain the serving cell, the workflow shown in the figure 3.8 is executed.

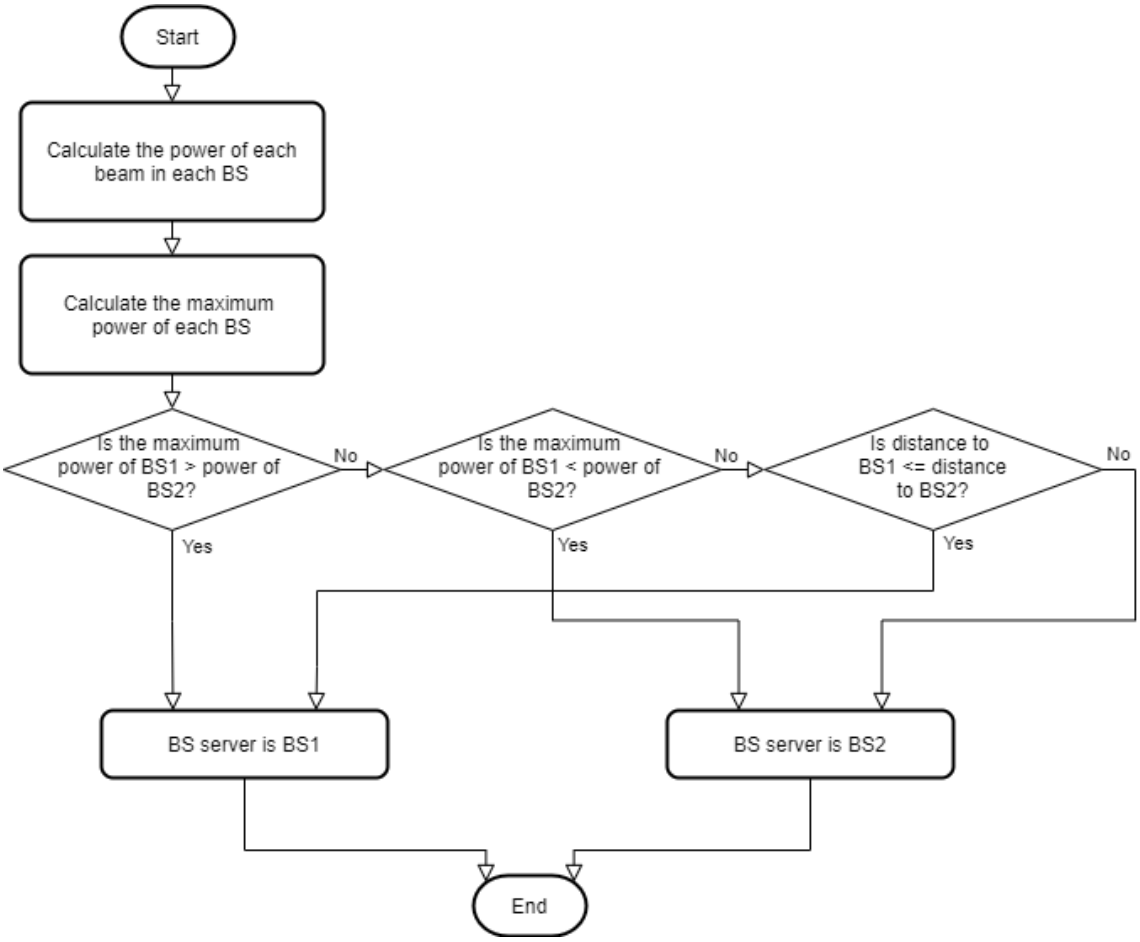

Figure 3.8: Serving Cell Workflow.

Once this procedure is executed, it is possible to know which base station best suits each location on the map, be it indoor or outdoor. Figures 3.9 and 3.10 show the serving cell for floor level locations. Again, BS1 in green (mostly on the left) and BS2 in yellow (mostly on the right).

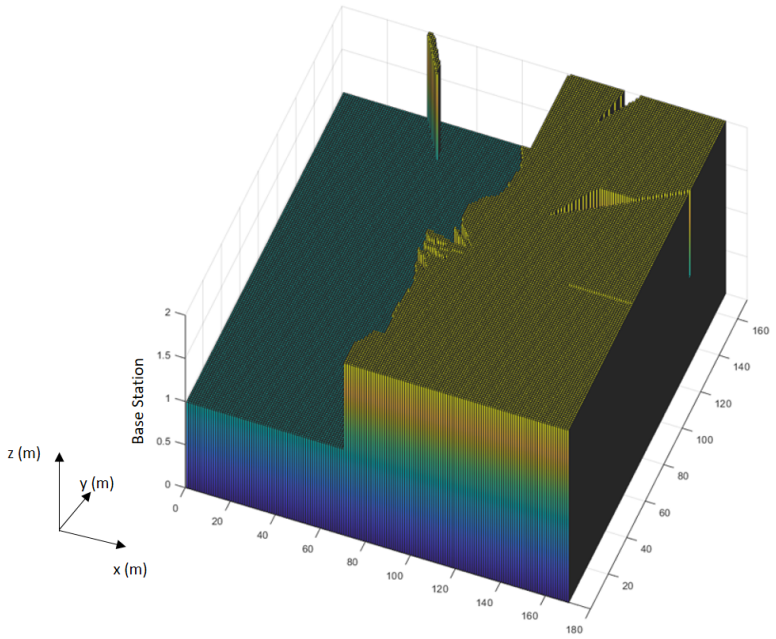

Figure 3.9: Serving Cell for each location of the map, at the ground floor (3D view).

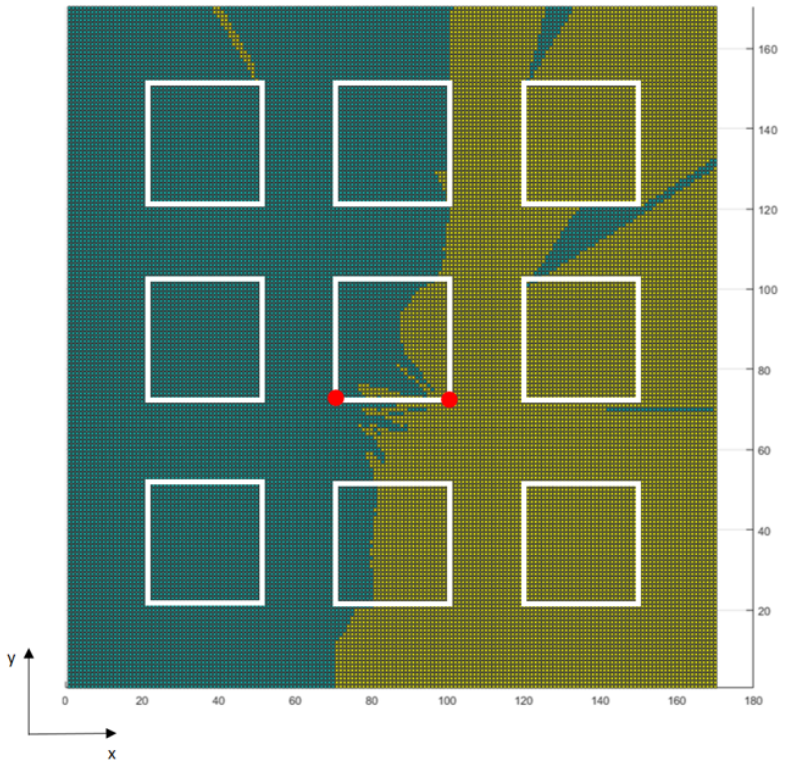

Figure 3.10: Serving Cell for each location of the map, at the ground floor (top view).

3.3.3 Beamforming

In order to understand how users are distributed among the various beams, it was calculated the number of admissible beams (that is, with acceptable power) in each position of the map, depending on the base station serving that location. Figure 3.11 presents the number of acceptable beams in each location, at ground level.

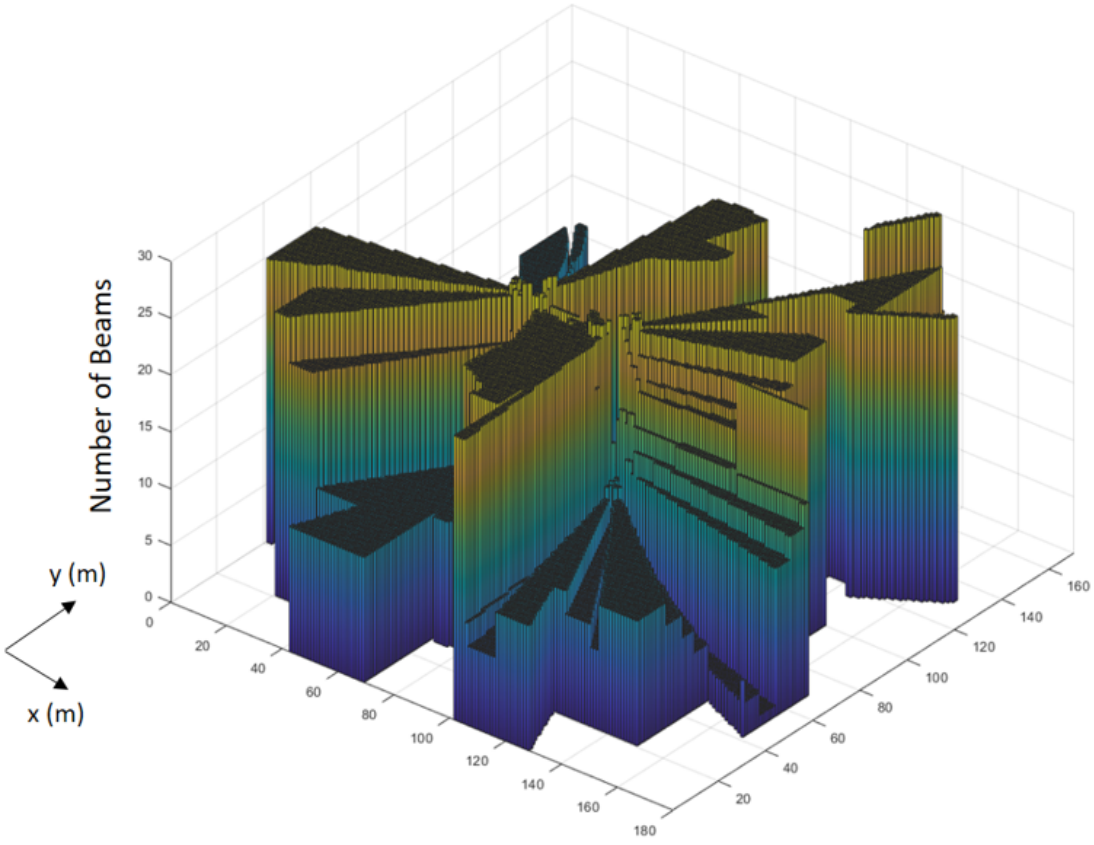

Figure 3.11: Number of acceptable beams in each location, at ground level.

Based on these calculations, the beam that provides the best quality of service to the end user is then chosen.

3.3.4 SINR

Once the value of the losses has been obtained and which base station serves each point on the map, it is now important to analyze each user individually. To do this, it is necessary to calculate the SINR of each user to subsequently validate whether or not to activate a new beam to provide service to that particular user.

There are only 3 possible chances at each base station: it has no active beams, it has an active beam, it has more than one active beam. For the first situation, without active beams, there is no signal interference caused by the serving cell (this study is not considering the interference that may exist between the various base stations) and, as such, the radio channel conditions in a UE is computed by the SNR:

$$\rho_N = P_{RX[dBm]} - N_{[dBm]} \tag{3.17}$$

being:

- P_{RX}: power in the receiving end of the connection;
- N: noise power, expressed in equation 3.18, where $PRBS_{max}$ corresponds to the maximum number of resource blocks available given the operating bandwidth and numerology. Bandwidths of 60 MHz and 100 MHz were used in the tested scenarios and, regarding numerology, it was used the numerology 1, with a Sub-carrier Spacing (SCS) equal to 30 kHz.

$$N_{[dBm]} = -174 + 10\log_{10}\left(\frac{BW_{[Hz]}}{PRBS_{max}}\right) + 7 \tag{3.18}$$

in the second and third situations mentioned above, when there is at least one active beam, the interference between beams starts to increase and, as such, it starts to affect the SINR values, and the more beams that are active the more influence it will have. After having the power associated with the best beam to serve a specific user and the interference associated with the various beams that may be connected, it is thus possible to calculate the SINR to each and every UE:

$$\rho_{IN} = P_{RX[dBm]} - I_{[dBm]} - N_{[dBm]} \tag{3.19}$$

being:

$I_{[dBm]}$: interfering power coming from the serving cell (sum of the power of each active beam with the exception of the one that is being considered):

$$I_{[dBm]} = \sum_{j=1}^{N} I_j - I_i \tag{3.20}$$

As an example, as previously done for path loss, an example of the SINR calculation is shown in the figure 3.12 for all positions on the map (considering that only each position is being served at each moment, that is, without interference), in order to verify that the SNR is much higher at base stations than at cell edge.

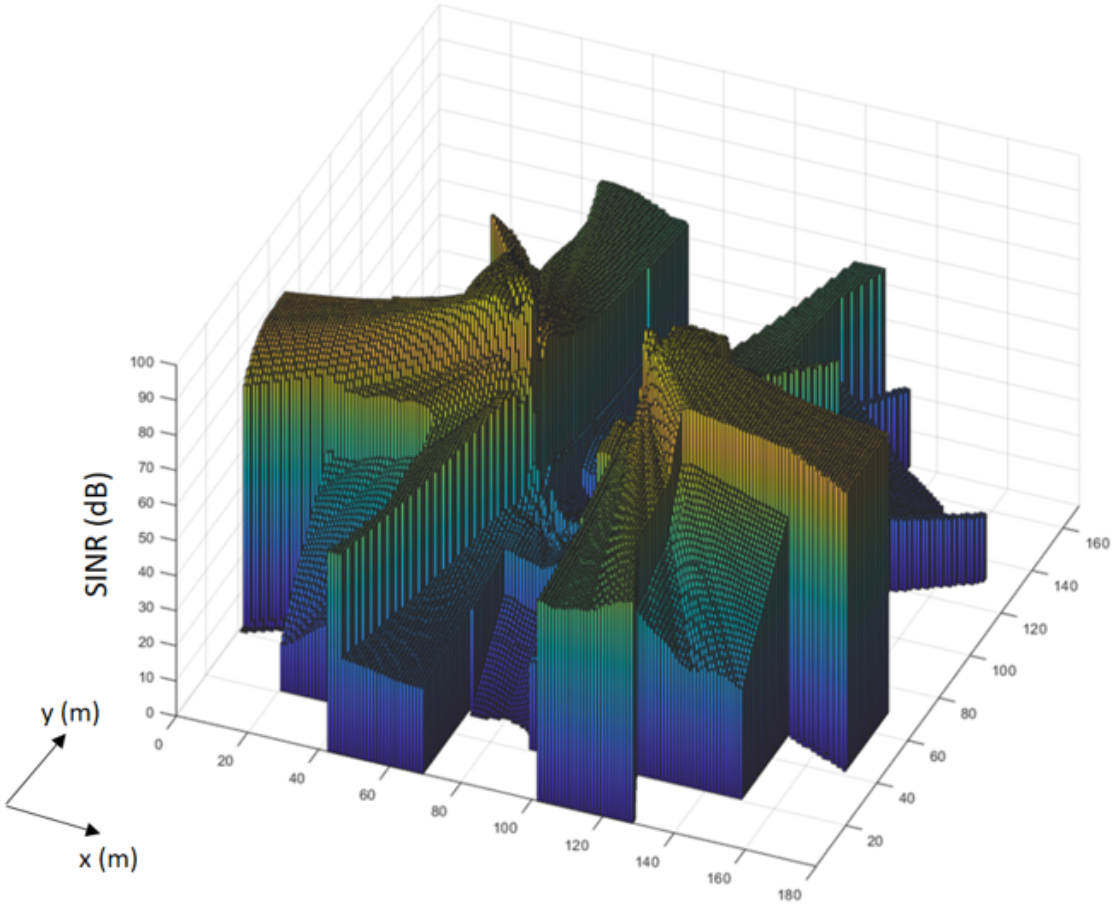

Figure 3.12: SINR for each location of the map, at the ground floor, without more users in the network.

3.3.5 Throughput

5G currently supports 5 types of modulations, shown in figure 3.13 but focus on Quadrature Phase Shift Keying (QPSK), 16-Quadrature Amplitude Modulation (QAM), 64-QAM, and 256-QAM.

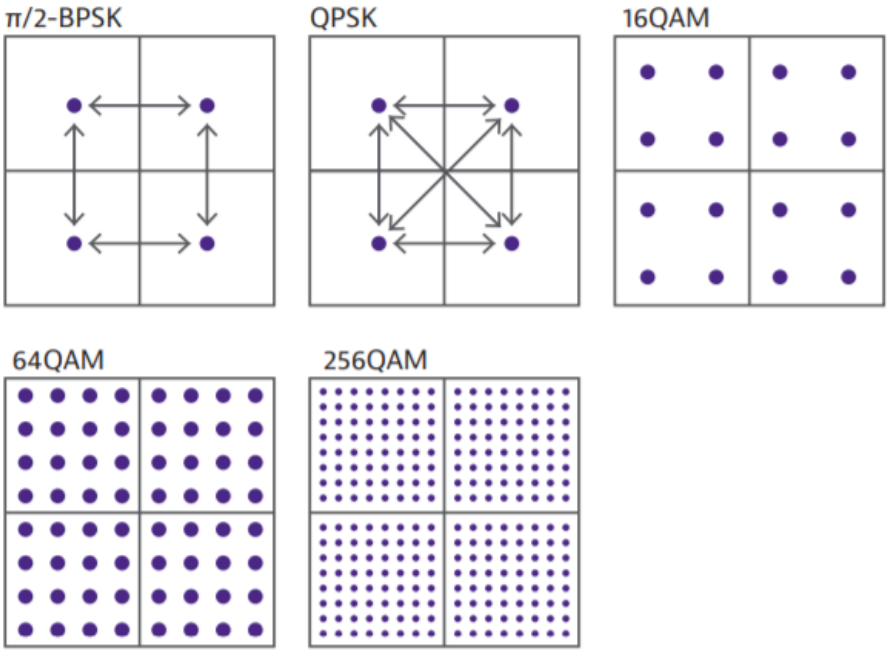

Figure 3.13: Constellation diagrams of the modulations supported in 5G

Using the work developed by [8], the relationship between SINR and throughput have to be considered in 4 different expressions for the downlink, one for each modulation. Each of these expressions is associated with the median value of the coding rate obtained from the Channel Quality Indicator (CQI) reported by the MT. The coding rates for these Modulation and Coding Scheme (MCS) no are presented in table 3.4.

Modulation	Target Coding Rate
QPSK	1/3
16-QAM	1/2
64-QAM	3/4
256-QAM	[0.7;0.9]

Table 3.4: Modulation Coding Scheme and its target coding rate.

Again, taking the work developed by [8], it was possible to obtain normalized curves for each of the modulations, thus adapting to the Vodafone Portugal settings. For a 2x2 MIMO channel and with a numerology 1 - SCS equal to 30 kHz - configuration, comes up:

For QPSK:

$$R_{b[bps]} = \frac{1.69748 \times 10^6}{14.0051 + e^{-0.577897 \cdot \rho_{IN}}} \tag{3.21}$$

For 16-QAM:

$$R_{b[bps]} = \frac{69019.7}{0.0926275 + e^{-0.295838 \cdot \rho_{IN}}} \tag{3.22}$$

For 64-QAM:

$$R_{b[bps]} = \frac{57416.6}{0.0220186 + e^{-0.24491 \cdot \rho_{IN}}} \tag{3.23}$$

For 256-QAM:

$$R_{b[bps]} = \frac{76559.2}{0.0178868 + e^{-0.198952 \cdot \rho_{IN}}} \tag{3.24}$$

In the figure 3.14 are shown these equations that allow do obtain the throughput per Physical Resource Block (PRB), after achieving the SINR of each user.

So, finally, the SINR limits of each modulation scheme are defined in table 3.5.

	QPSK	16-QAM	64-QAM	256-QAM
ρ_{min} [dB]	-10	2.45	8.75	18.10
ρ_{max} [dB]	2.45	8.75	18.10	45
$\rho_{interval}$ [dB]	12.45	6.35	12.6	26.9

Table 3.5: SINR limits per modulation.

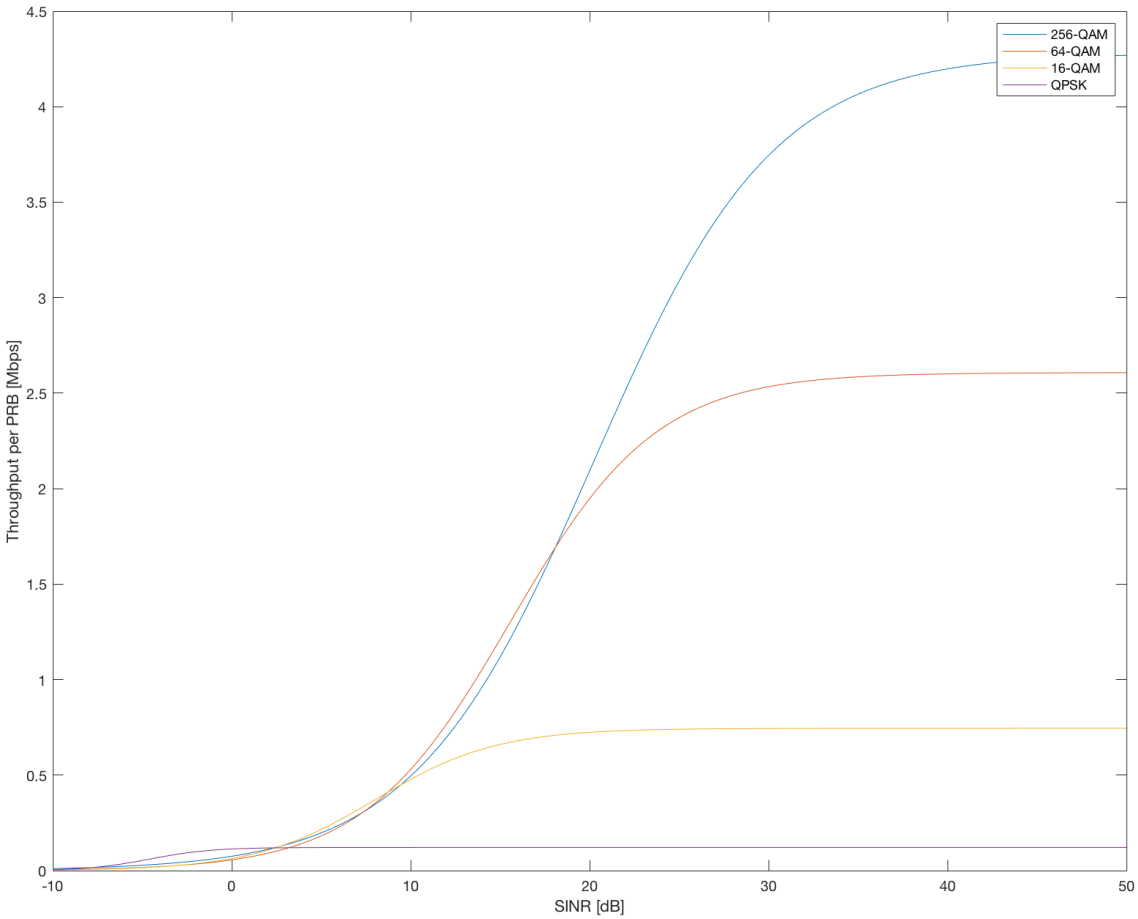

Figure 3.14: Throughput per PRB, after achieving the SINR of each user (extracted from [8]).

4

Results Analysis

Contents

To assess the performance of this simulator, this chapter presents an analysis of the data taken from the simulator, as well as the data collected from the Vodafone Portugal live network.

Starting with a brief description of the conditions under which the measurements were made on the live network, going through the settings that were applied on the network, the functionalities of the terminal and the results themselves. As stated before, bandwidths of 60 MHz and 100 MHz and the numerology 1, with a SCS equal to 30 kHz, were used in the tested scenarios.

4.1 Setup Configuration

The phone used to perform some tests in the live network environment was a Xiaomi Mi 10, running Android 10, which supports the following mobile network technologies: 2G, 3G, 4G and 5G.

The table 4.1 indicates which bands of each mobile network technology are compatible with the referred terminal. In addition, it also supports 4x4 MIMO and Higher Order Diversity.

Technology	Division Duplex Mode	Bands
2G	FDD	B2, B3, B5, B8
3G	FDD	B1, B2, B4, B5, B8
4G	FDD	B1, B2, B3, B4, B5, B7, B8, B20, B28, B32
4G	TDD	B38, B40
5G	TDD	B1, B3, B7, B28, B77, B78

Table 4.1: Mobile network bands supported by Xiaomi Mi 10 (extracted from [11]).

The Vodafone Portugal live network present in this location includes several sectors to offer coverage in the referred area and, as such, it is necessary to explore the various sectors in detail in this study.

To establish a connection to the 5G live network, the terminal connects to the 4G network and, if that cell is an anchor of the 5G technology, the process of trying to establish a connection to a 5G cell begins.

In the scenario in which the tests were carried out, it was possible to have a slightly more advanced configuration in which a 4G cell could be an anchor cell of several 5G cells and, simultaneously, a 5G cell could have several 4G anchors. Through this process, it was possible to establish 5G connections using 4G anchor cells that were not colocalized.

Each corner of the headquarters building has a 4G sector, as shown in figure 4.1. The 2 corners of the building that also have a 5G sector are shown in figure 4.2, on top of the 4G ones. Each of these figures also has the Physical Cell Identifier (PCI) indication of the various cells.

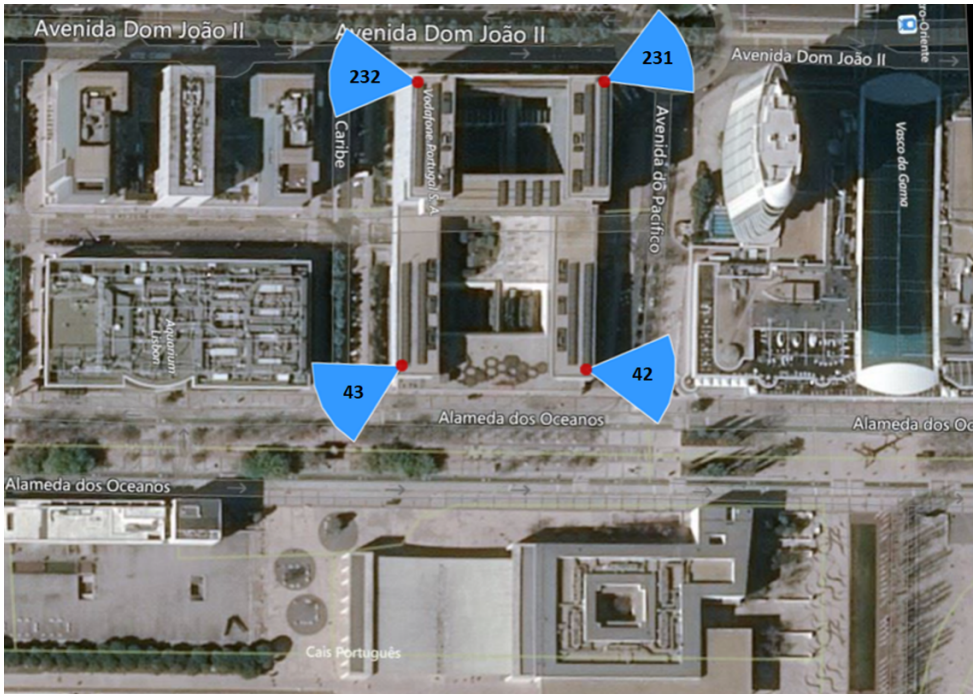

Figure 4.1: Sector locations and PCI of the 4G the live network

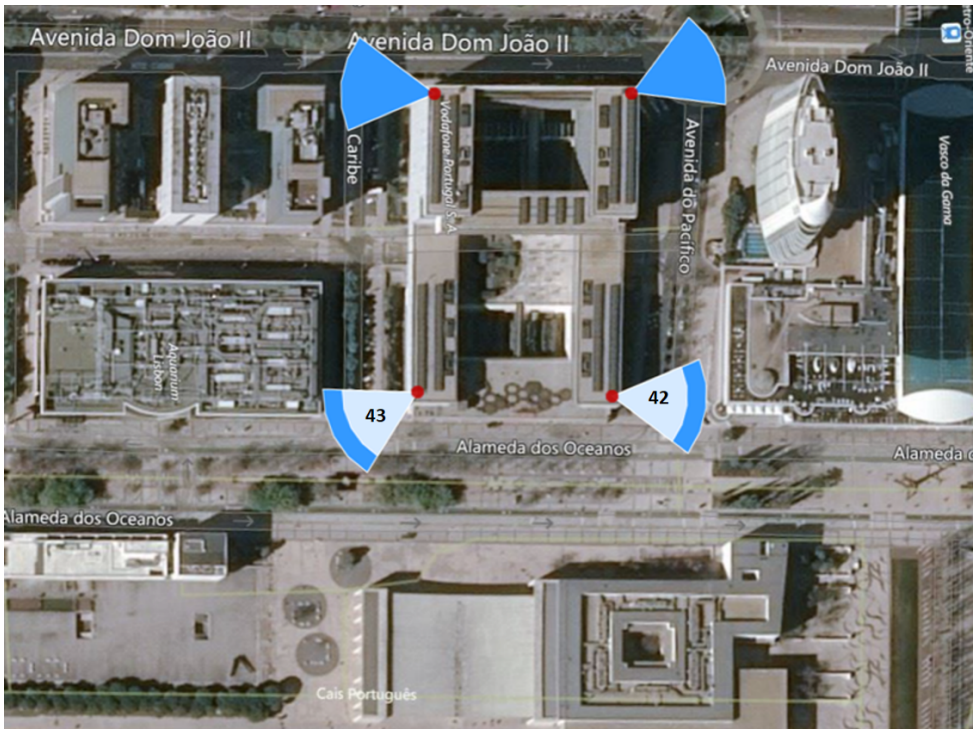

Figure 4.2: Sector locations and PCI of the 5G live network

4.2 Walk-test Results and Analysis

The tests on the 5G network were carried out on a summer day in 2020, with clear skies and temperatures around 30 degrees Celsius, in some previously selected locations. The basic criterion for selecting these 59 locations was to try to take advantage of the symmetry that exists in the block, without affecting the number of locations to perform data collection nor negatively impact the collection of the various types of scenarios possible in the area.

In order to ensure similar conditions in all tests, an effort was made to try to maintain the distance to the buildings at locations that were located close to buildings. It is also important to note that all locations are outdoor since, unfortunately, due to the situation of Covid-19, there were several restrictions to access indoor environments in the area, not allowing indoor testing.

Due to the limitations of data collection from the walktests, it was not possible to obtain the power values received at the terminal, therefore, this analysis will not be performed in this comparison.

Thus, the locations selected to collect data are shown in the figure 4.3.

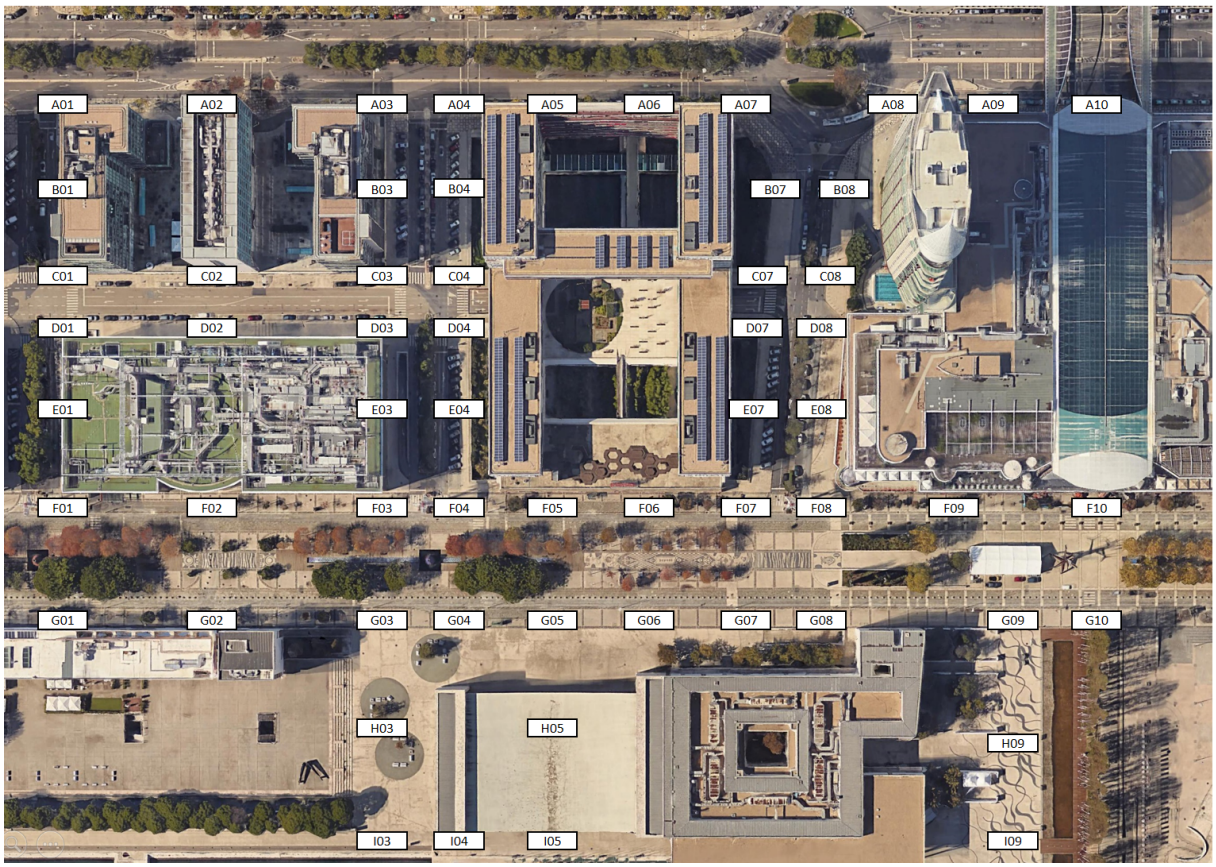

Figure 4.3: Real map of Vodafone headquarters surroundings with tested locations

Given the limitations of the type of simulator that was used, it was not possible to accurately transpose all real locations to the simulator. The figure 4.4 shows the locations chosen in the simulation environment. A scale is displayed on the right, indicating the height of the various buildings (in number of floors).

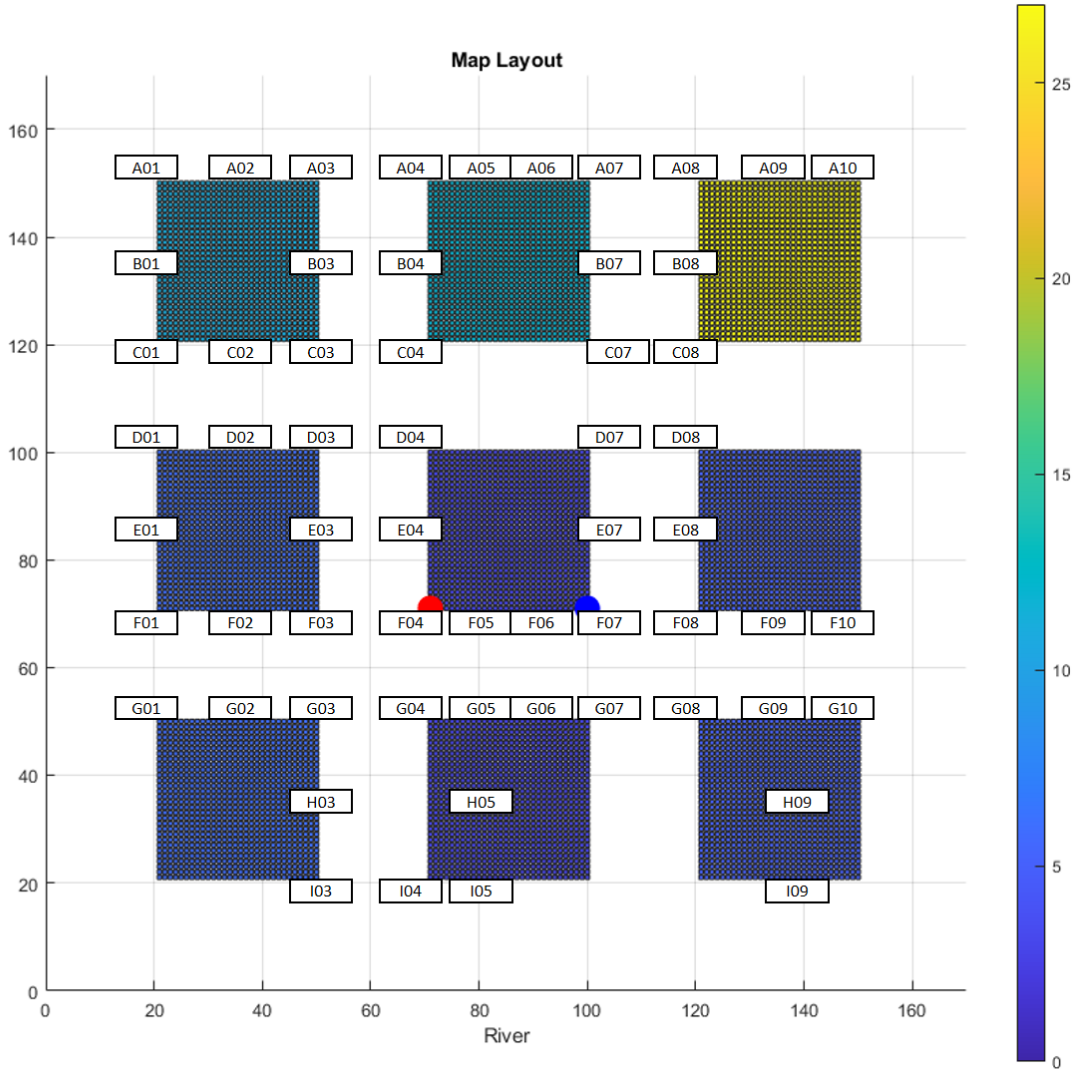

Figure 4.4: Simulator map of Vodafone headquarters surroundings with tested locations

As can be seen when comparing the figures 4.3 and 4.4, there are locations that in a real environment are outdoor but in the simulator are considered indoor (locations H09 and I09). The H05 location is considered indoor in the simulator but in real life it is an outdoor location with a roof. Finally, the building visible in the lower left corner of the simulator map is actually an outdoor space so any collection and subsequent comparison could be dubious.

The simulator considers the existence of the 2 base stations 5G: the base station 1, on the left and in red in the figure 4.4, and the base station 2, on the right and in blue in the same figure.

Running the simulator for the locations mentioned above, it appears that the distribution of the locations by the base stations is not done equally by the two stations. The figure 4.5 shows the number of locations covered by each base station.

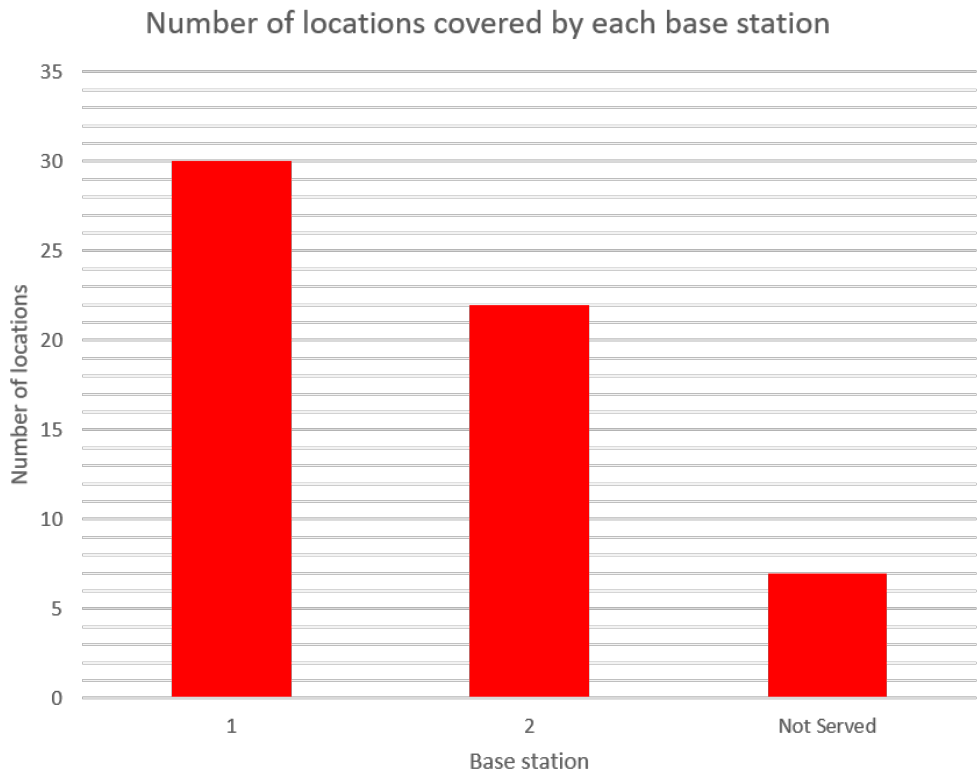

Figure 4.5: Number of locations covered by each base station

Thus, according to the simulator, base station 1 is responsible for covering 30 locations, base station 2 for 22 locations and there are 7 locations that do not have coverage from any of the 2 base stations.

To validate whether this distribution of locations of possible user terminals was adjusted to reality, the PCIs to which the test terminal connected in a real environment at each location were collected. The distribution of 4G and 5G Physical Cell Identities during trials is presented in figure 4.6.

In order to compare the real 5G cells with those of the simulator, the cell with PCI 43 corresponds to base station 1 of the simulator and the cell with PCI 42 corresponds to base station 2.

In addition, the 4G real cells are also presented: cells with PCI 42 and 43 colocalized with 5G and cells with PCI 231 and 232 located at the other end of the building. Two other cells were also detected with PCI 69 and 160 but that were not anchors of any of the two 5G cells under analysis in the study.

From the figure 4.6, it can be seen that most 5G data sessions were anchored by the colocalized 4G

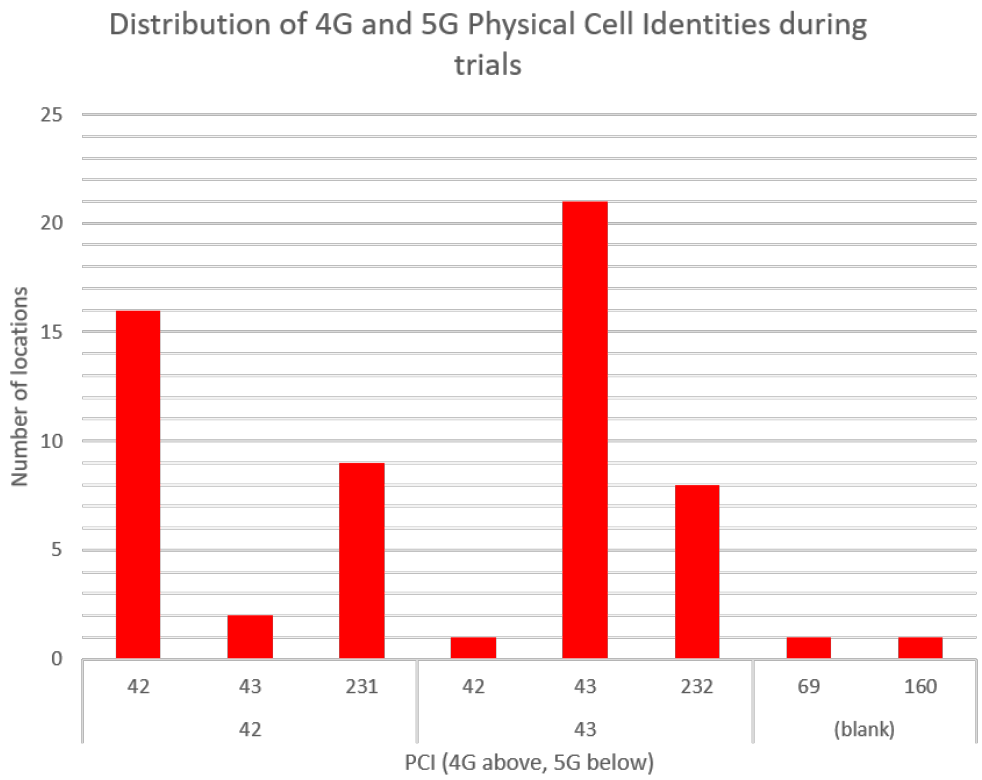

Figure 4.6: Distribution of 4G and 5G Physical Cell Identities during trials

cell. In some cases the 4G anchor was one of the other cells that did not have 5G in that sector. As previously mentioned, in the test scenario any of the 4G cells with the PCI 42, 43, 231 and 232 could be anchors of the 5G cells with the PCI 42 and 43. It was found that the handovers between these 4G stations were carried out according to the best coverage conditions, as expected, and without causing problems in the 5G connection. In 2 particular locations it was not possible to do a 5G data session since the 4G cell was not the anchor of any 5G cell.

It should also be noted that, as predicted in the simulator, the 5G base station with PCI 43 (equivalent to base station 1 in the simulator) covers more locations than the base station with PCI 42 (equivalent to base station 2 in the simulator)

After analyzing the group of locations covered by each 5G base station, there is a need to know which beam of each base station covers each location. As mentioned in the previous chapter, the beam of each station covering a given location is chosen based on the value of its gain and its direction. As it was not possible to collect this information from the live network, it is shown in figure 4.7 the number of locations served by specific beams. Figures 4.8 and 4.9 also show which beam, from base station 1 and 2, respectively, which covers each location.

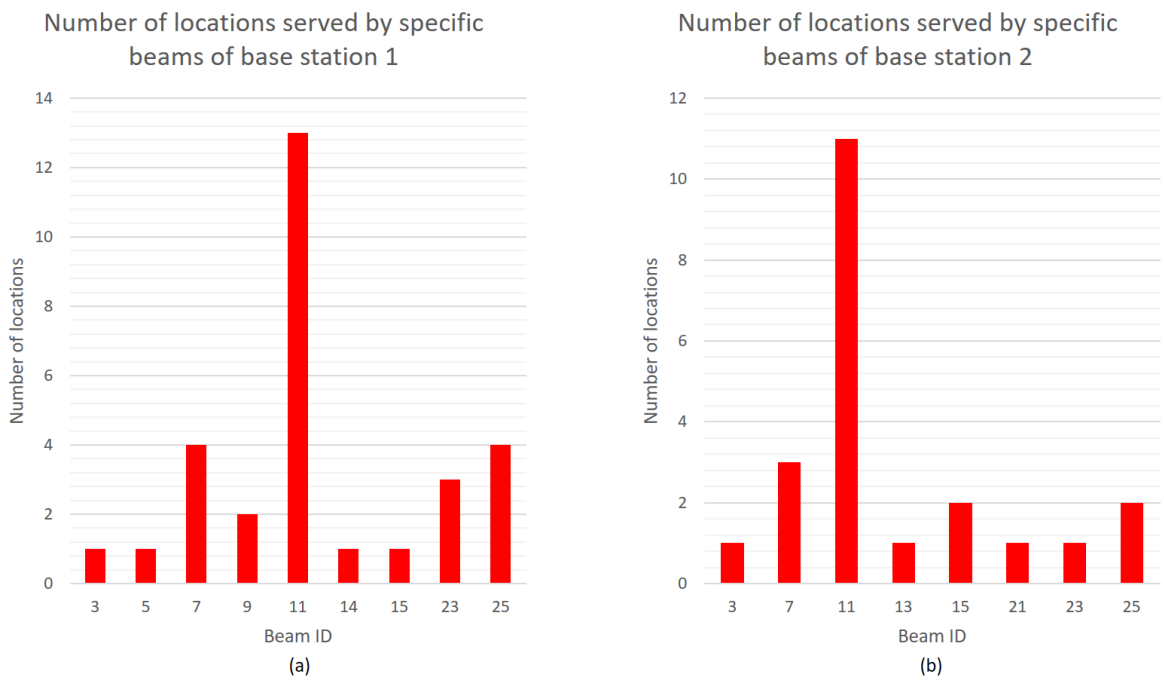

Figure 4.7: Number of locations served by specific beams of base station 1 (a) and 2 (b)

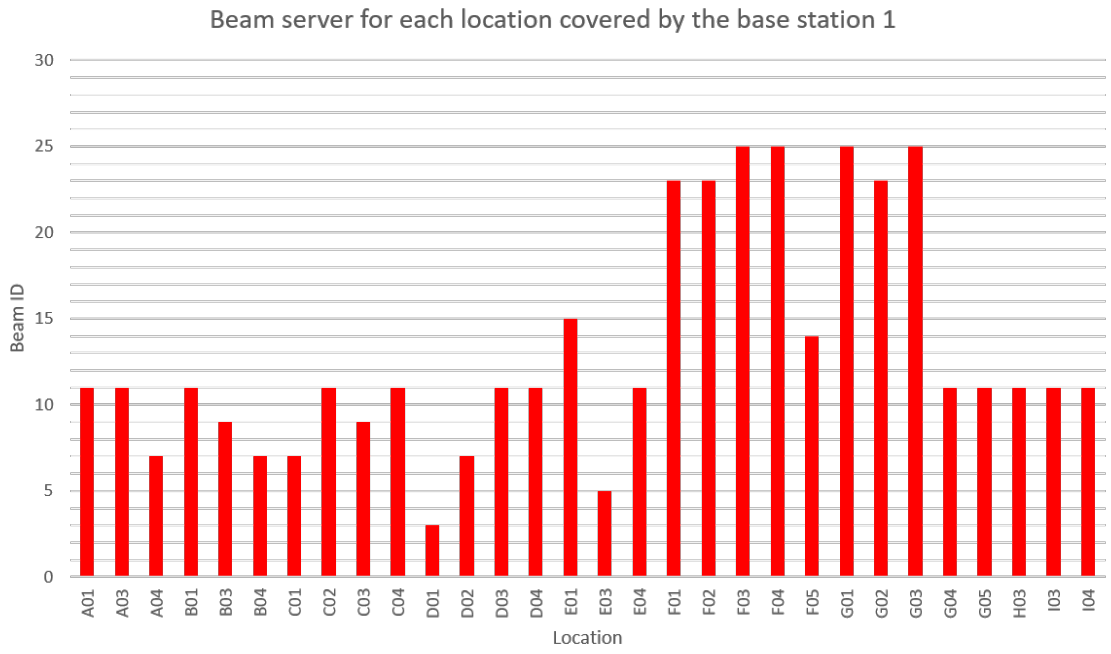

Figure 4.8: Beam server for each location covered by the base station 1

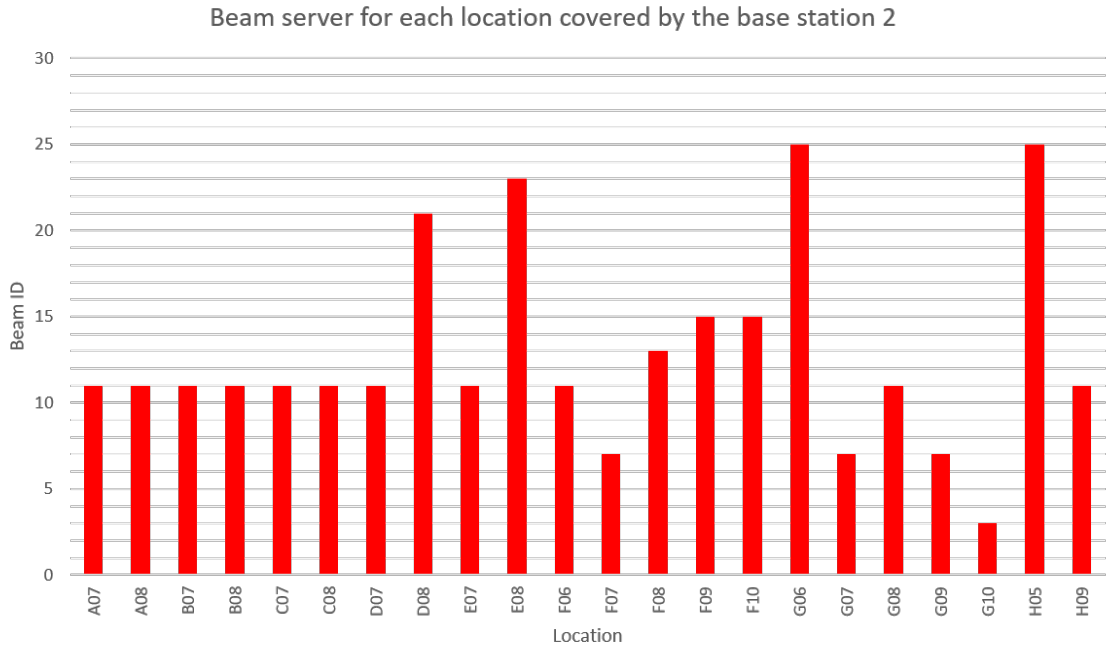

Figure 4.9: Beam server for each location covered by the base station 2

From the analysis of these figures, the beam with the ID 11 stands out as the beam that covers more locations in both base stations, resulting in 13 locations covered by base station and 11 locations covered by base station 2.

The users, present in the referred locations, are distributed in the simulator by the various beams following the criteria mentioned in the previous chapter. In the real network it is not possible to know how this distribution is made since the provider's algorithm is proprietary, that is, it is not public.

With the referred beams from the 2 base stations, it is possible, according to the simulator, to cover users with an acceptable speed. The figure 4.10 shows the throughput in each UE location covered by base station 1, in a 60 MHz setup and figure 4.11 shows the ones covered by base station 2, in the same conditions.

Likewise, running the simulator and repeating the walk-tests with the base stations configured with a bandwidth of 100 MHz, the figures 4.12 and 4.13 are obtained. It is important to note that when the walk tests were performed, there was a limitation on the network that did not allow speed tests above 970-1000 Mbits. Thus, these figures must be analysed with particular care since, once this problem is overcome, it is expected that the speeds will approach the theoretical values obtained by the simulator.

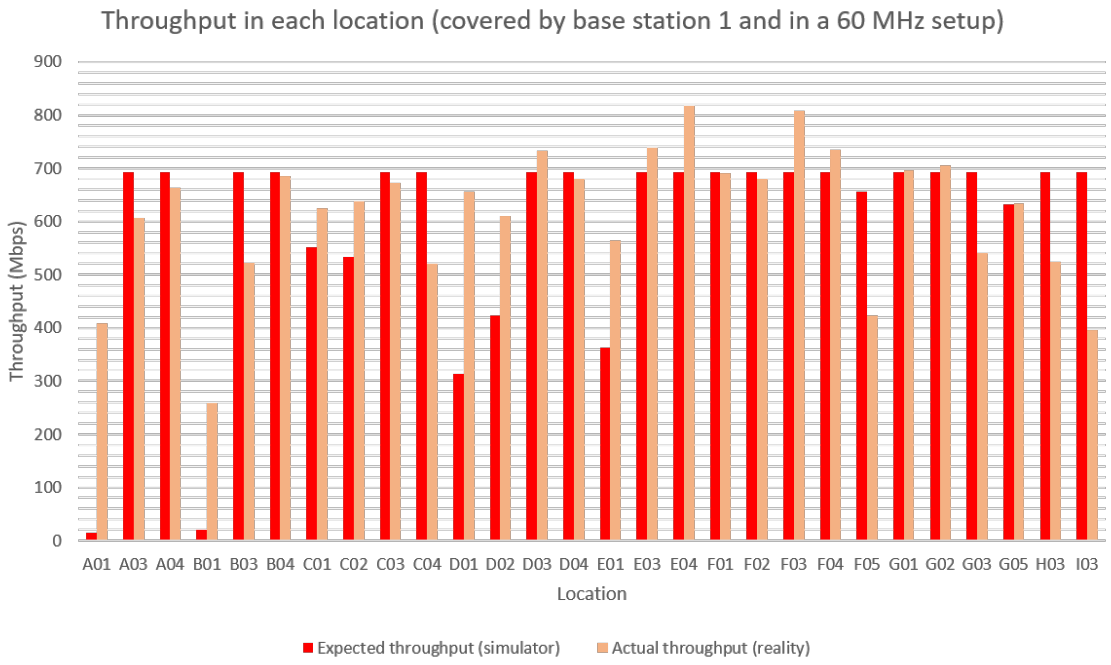

Figure 4.10: Throughput in each location (covered by base station 1 and in a 60 MHz setup)

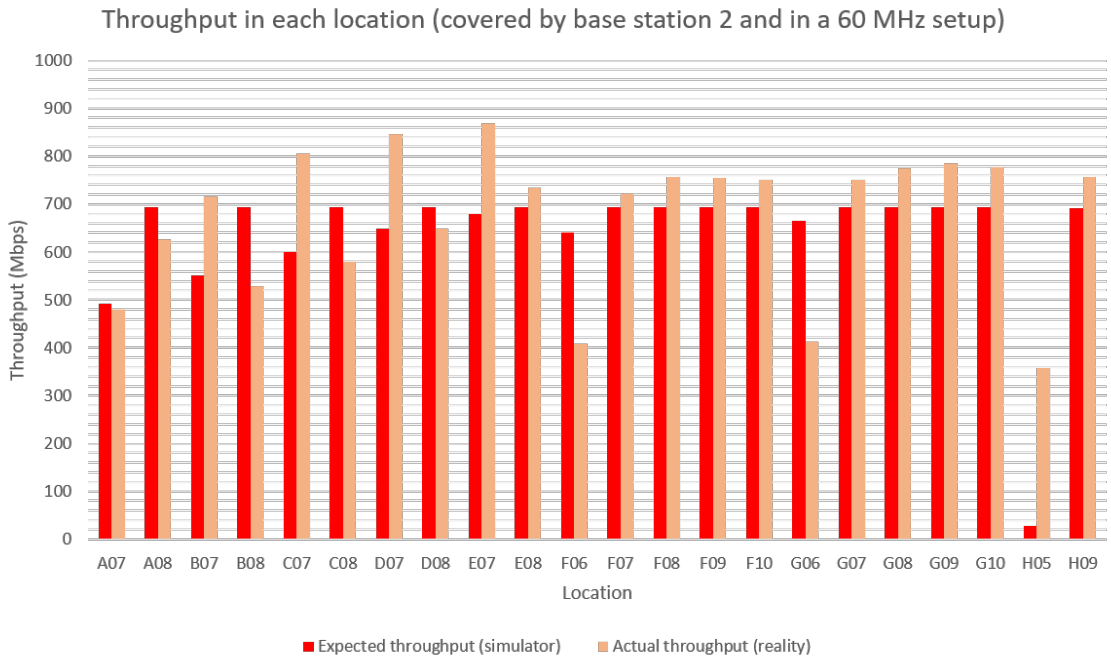

Figure 4.11: Throughput in each location (covered by base station 2 and in a 60 MHz setup).

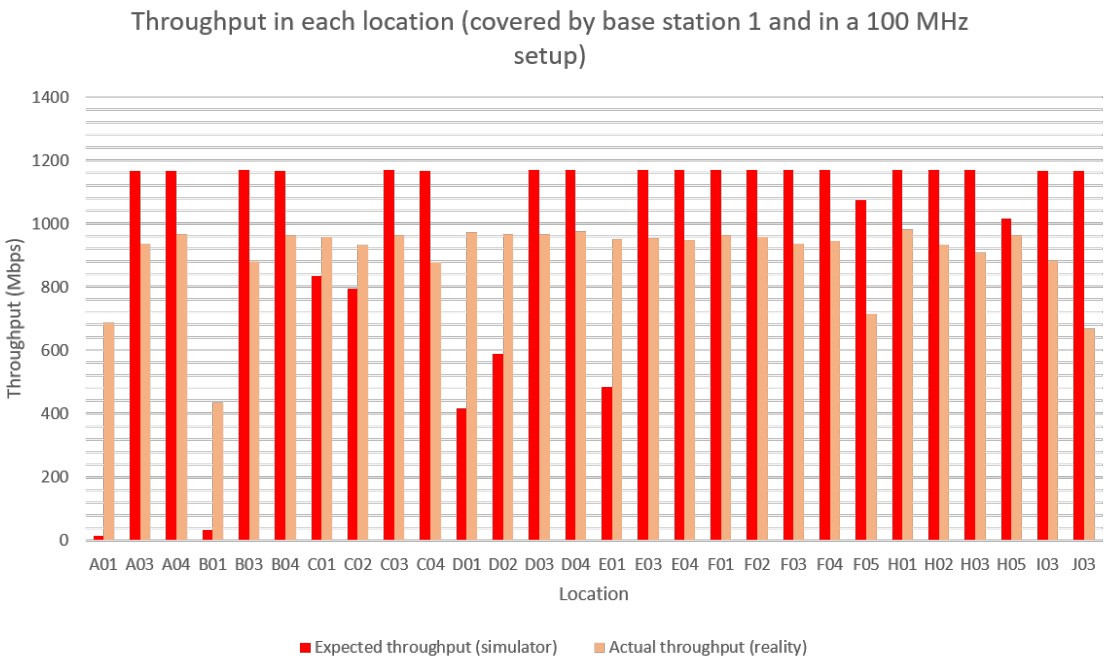

Figure 4.12: Throughput in each location (covered by base station 1 and in a 100 MHz setup).

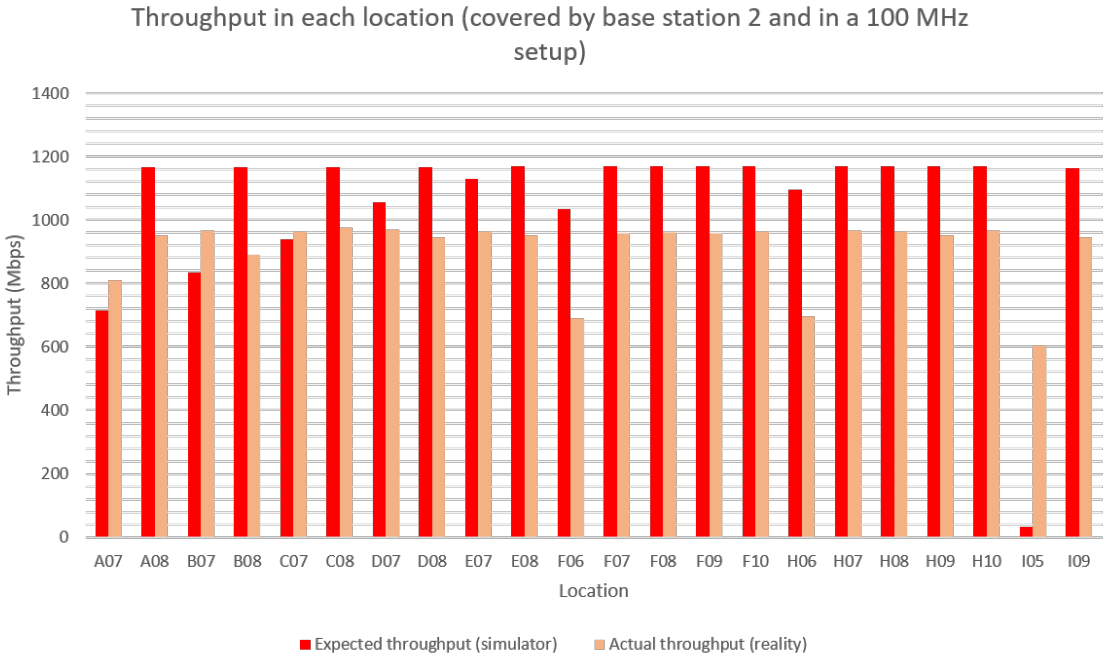

Figure 4.13: Throughput in each location (covered by base station 2 and in a 100 MHz setup).

Comparing the figures referring to the configurations with a bandwidth of 60 MHz with those of a bandwidth of 100 MHz, it can be seen that the chart behaviour is quite identical. With the exception of the aforementioned limitation, the speeds in the tests are proportional, which would be expected because the propagation conditions were maintained. The figure 4.14 shows the average speed values obtained in each of the locations served by the two base stations and in each scenario, either with a bandwidth of 60MHz or with a bandwidth of 100 MHz.

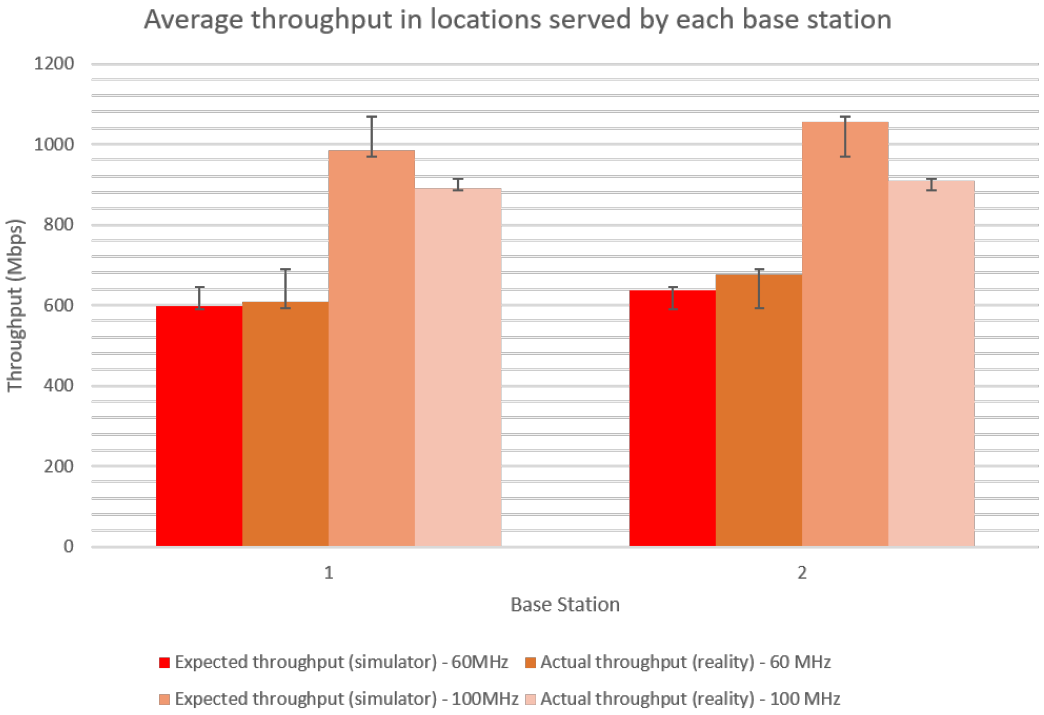

Figure 4.14: Average throughput in locations by each base station.

It appears that there is some differences between the estimated and actual values. On the one hand, in the case of 60 MHz, the average of the actual values is slightly above the average of the values estimated by the simulator. On the other hand, in the case of 100 MHz, the average of the actual values is well below the estimated values due to the limitation already addressed. These differences are also strongly related to the location of the terminals on the map since there are positions that may not be fully mapped due to the irregularities of the surrounding scenario.

In order to understand the discrepancy between the simulator values and the real values, the figure 4.15 shows the error values obtained between the measured values and the simulated values, calculated according to the equation 4.1.

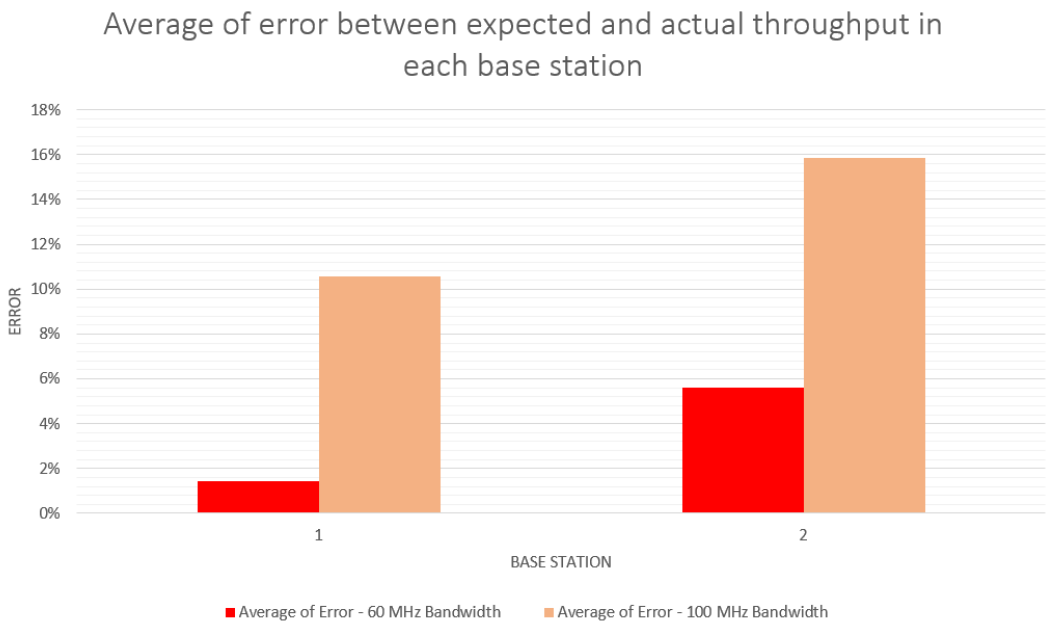

Figure 4.15: Average of error between expected and actual throughput in each base station.

$$Error(\%) = \frac{|RealValue - SimulatedValue|}{RealValue} \times 100\% \tag{4.1}$$

Despite having some samples with low values for station 1 and others with higher values for station 2, it appears that the error between the simulated values and the real values, compared to the real values, is still a little high. In the case of 60 MHz there is an error of about 1,5% at base station 1 and 5,5% at base station 2. In the case of 100 MHz there is an error of about 10,5% at base station 1 and 15,8% at base station 2. As an example, the figures 4.16 and 4.17 show the effective difference between the 2 types of values for the case with 60 MHz.

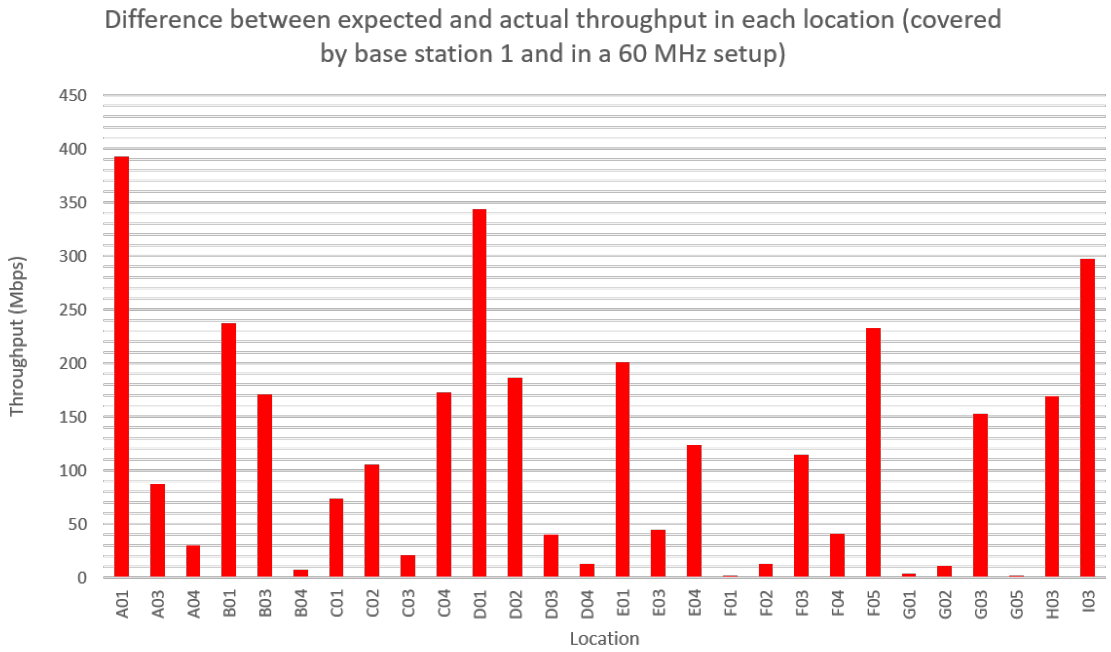

Figure 4.16: Difference between expected and actual throughput in each location (covered by base station 1 and in a 60 MHz setup)

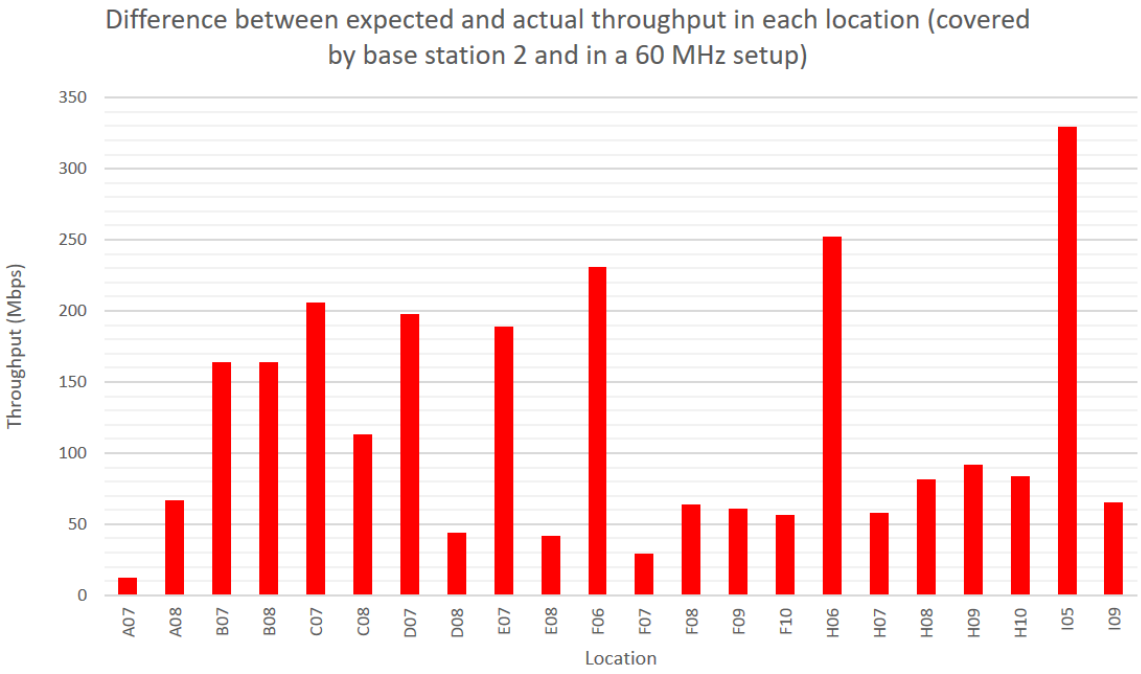

Figure 4.17: Difference between expected and actual throughput in each location (covered by base station 2 and in a 60 MHz setup)

4.3 Case with 100 UEs in random locations

This section tests a hypothetical scenario with random locations but with one criterion: 20% of users are in an outdoor environment, on the ground, and 80% are in an indoor environment, spread over the various floors of the buildings. The figure represents the beam that serves the locations of the users in an outdoor environment since, as users are distributed in 3 dimensions, it is difficult to represent users in an indoor environment.

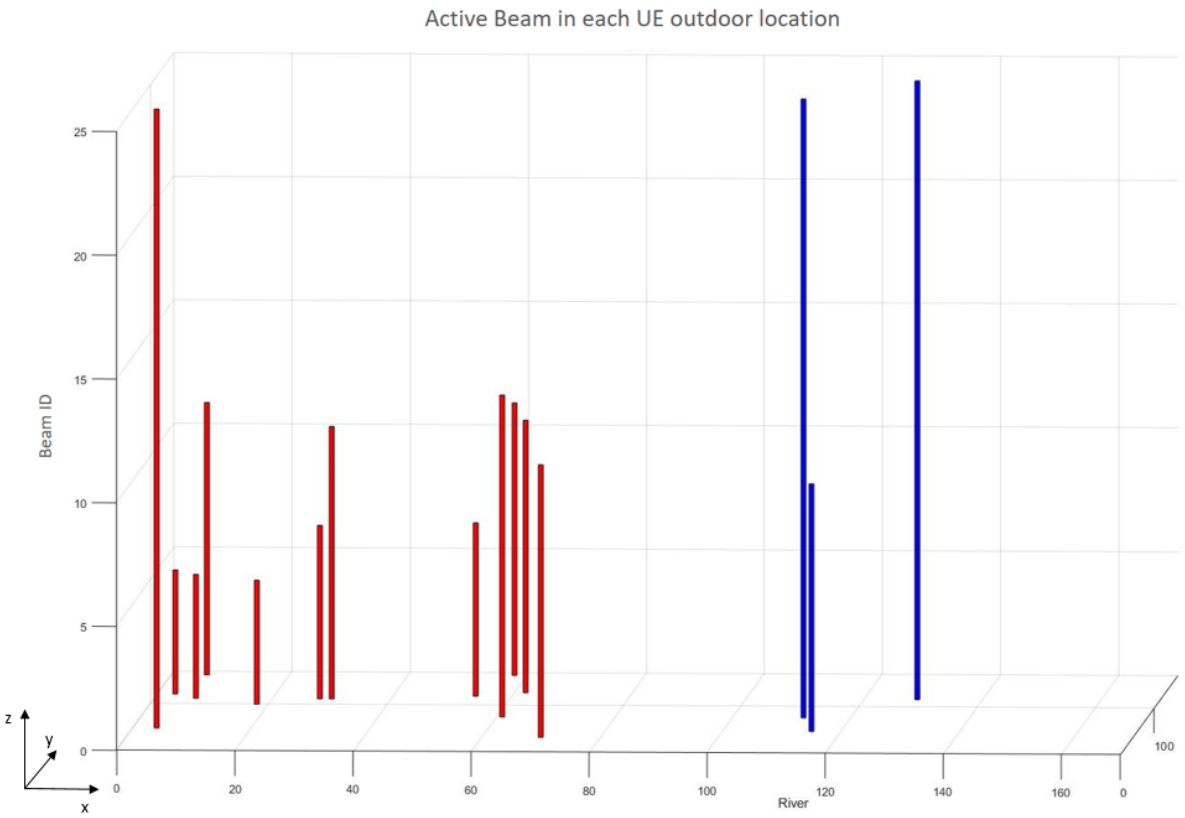

Figure 4.18: Active Beam in each UE outdoor location (BS1 in red, BS2 in blue).

In order to overcome this limitation of representing all UEs in a single figure, there is a need to check how many beams are active and how many users are served by each of the beams of each base station. The figure 4.19 represents precisely that.

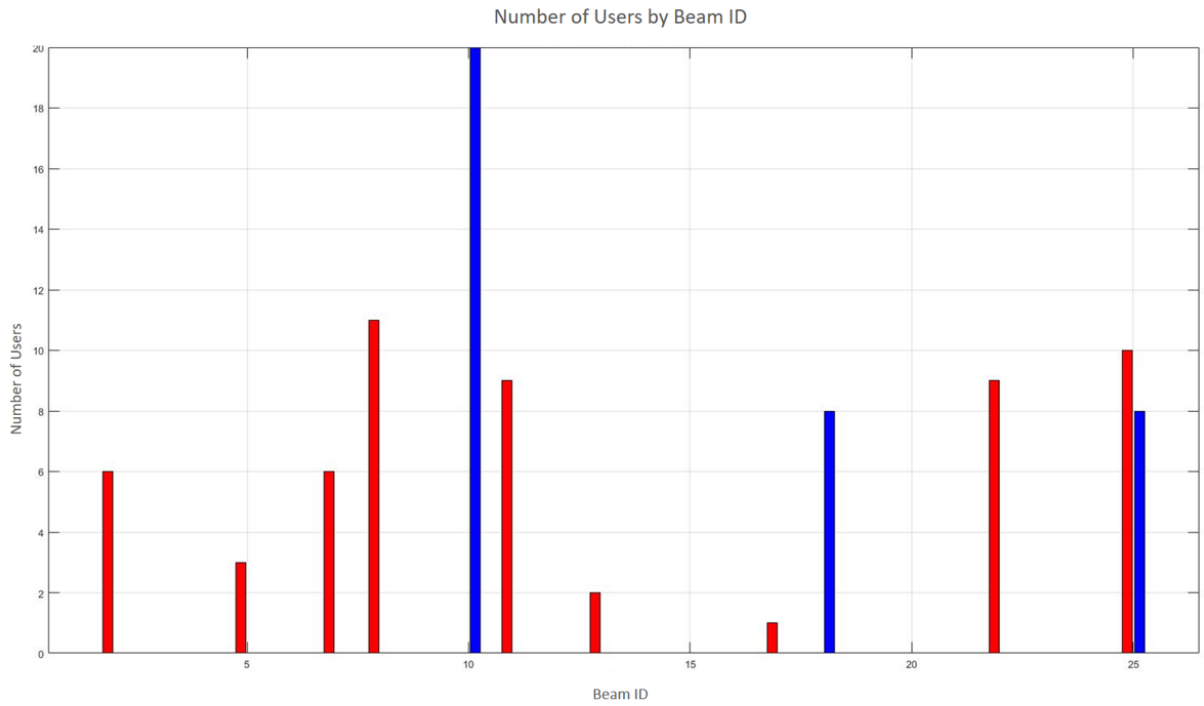

Figure 4.19: Number of users served by each Beam ID (BS1 in red, BS2 in blue).

Base station 1 is used to serve 51 users and has 9 active beams, while base station 2 is used to serve 28 users and has 3 active beams, as shown below in table 4.2.

Base Station	Beam	Number of PRBs	Number of UEs	Number of PRBs per UE
1	2	162	6	27
1	5	162	3	54
1	7	162	6	27
1	8	160	10	16
1	11	160	8	20
1	13	162	2	81
1	17	162	1	162
1	22	162	9	18
1	25	162	6	27
2	10	154	14	11
2	18	160	8	20
2	25	162	6	27

Table 4.2: Beam and PRB usage.

In base station 1, the percentage of served users is 86.44 %, the number of PRBs used in BS is 1454 PRBs, the percentage of PRBS used : 99.72 % and the average number of PRBs per beam : 162 PRBs. In base station 2, the percentage of served users is 68.29 %, the number of PRBs used in BS is

476 PRBs, the percentage of PRBS used is 97.94 % and the average number of PRBs per beam : 159 PRBs.

Regarding throughput, the figure 4.20 presents it and the location of the users, in X and Y coordinates only, without indicating the height, in order to have a perception of the distribution of users on the map.

Figure 4.21 represents throughput values for each user using base station 1 and, likewise, the 4.22 represents throughput values for base station 2.

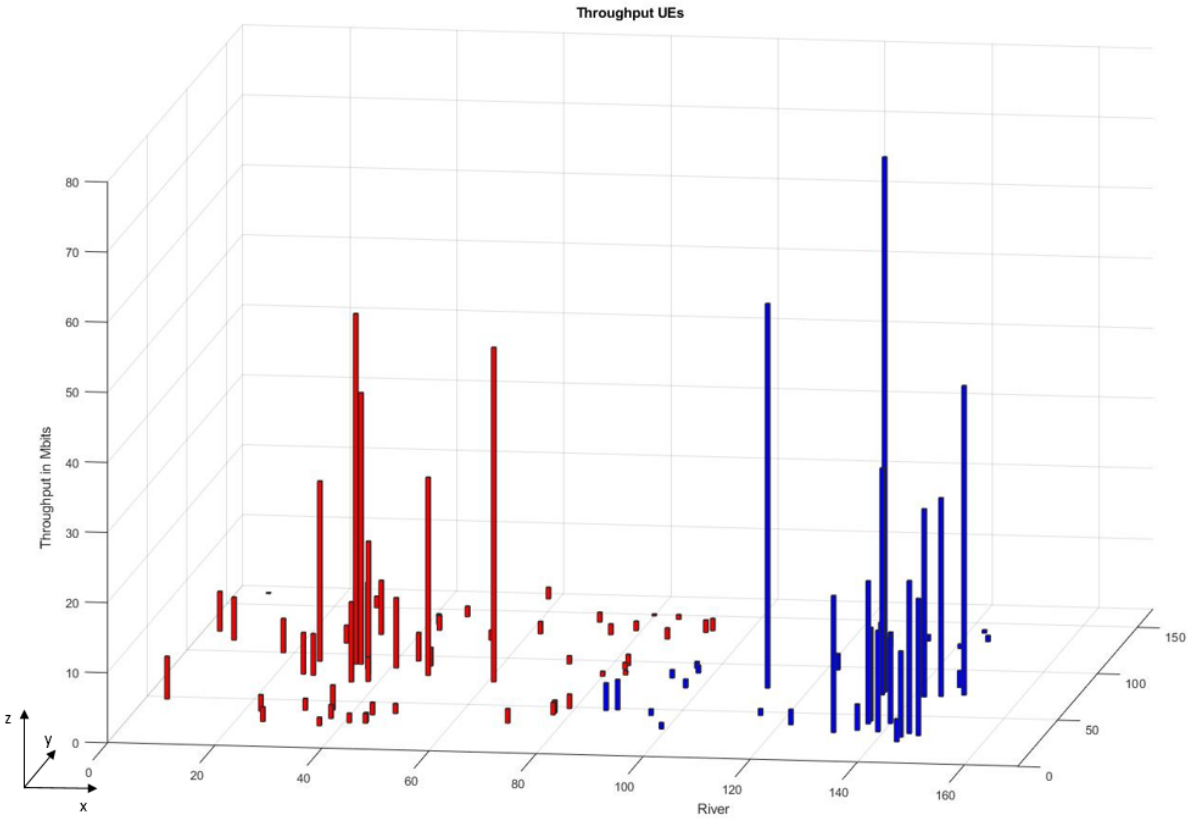

Figure 4.20: Throughput and the location of the users in the map.

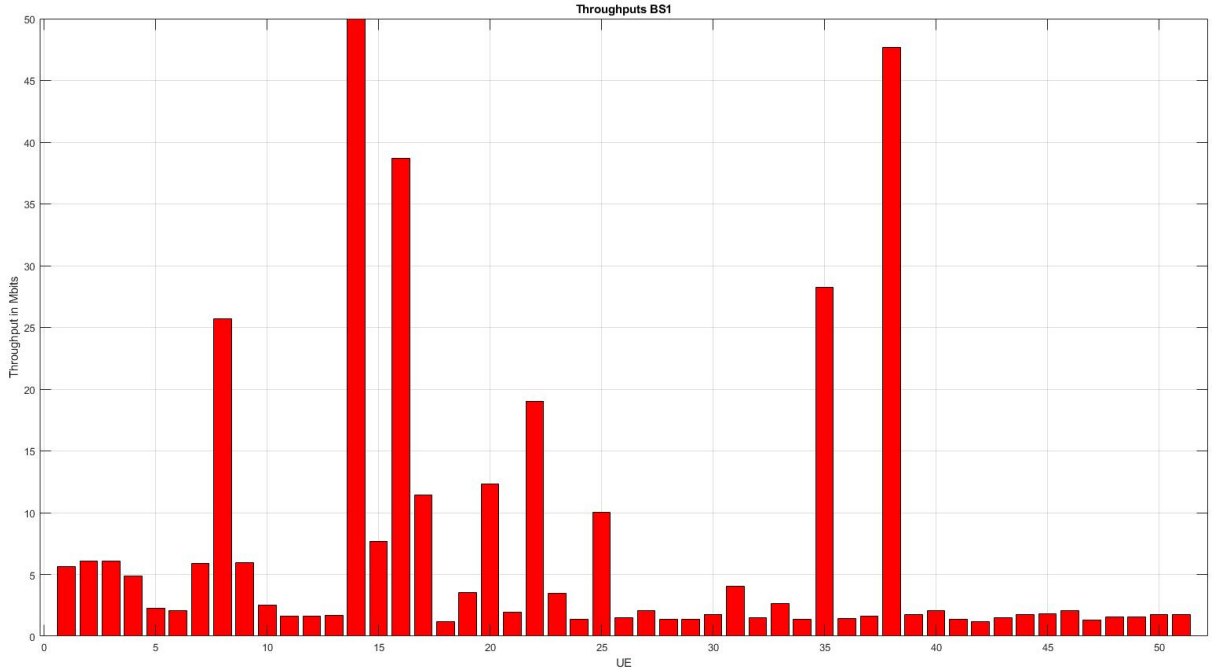

Figure 4.21: Throughput for each UE served by base station 1.

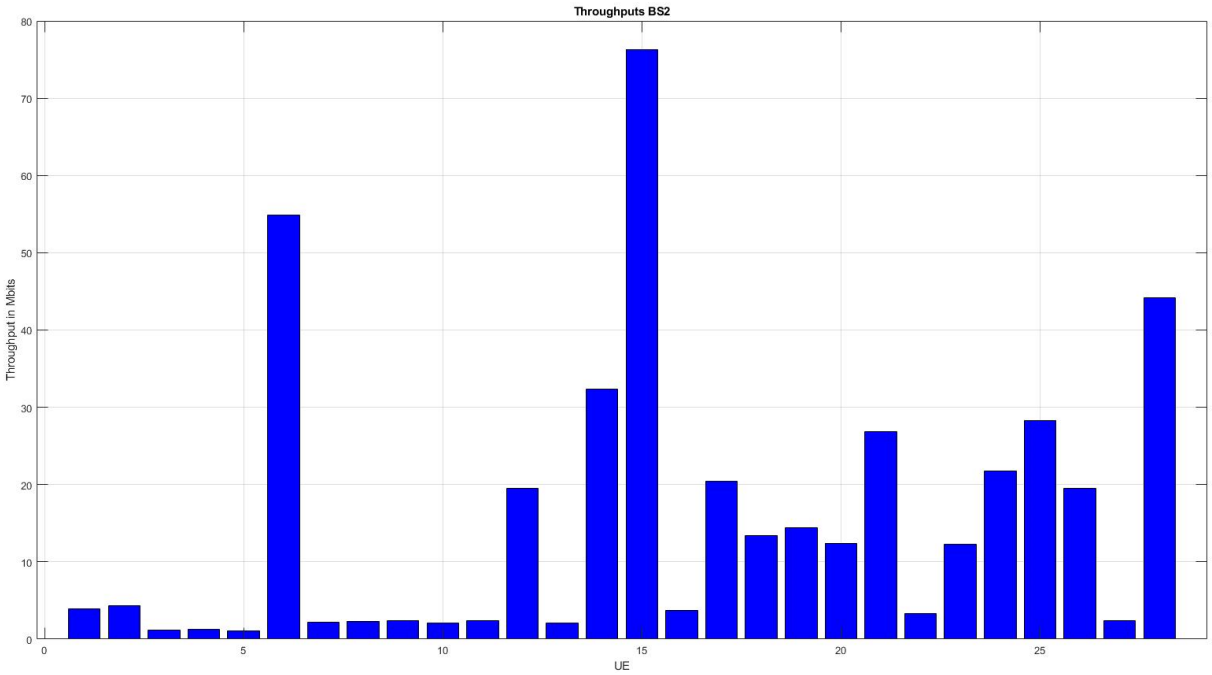

Figure 4.22: Throughput for each UE served by base station 2.

5

Conclusions and Future Work

This document describes the work developed for the Master Thesis in in Electrical and Computer Engineering. Firstly is presented an overview of the main theme, 5G, and the motivation that led to the proposed work. Since the main task of this thesis was to study the impact of the beamforming technology in 5G mobile networks, it was crucial to carry out an in-depth study of 3 major themes: LTE, NR and beamforming. It was found from the beginning of the project that to make a correct coverage comparison between LTE and NR 3500 MHz, several aspects such as the location of the base stations and the test environment have to be considered.

As described in this document, it was possible to implement a simulator that estimates the coverage and capacity of the network environment of the Vodafone Portugal headquarters building. Using the gains of the antenna model used and calculating the path loss between the locations of the serving cell and the various UEs, it was also achievable to create a model that indicates which beam serves each user and present an estimate for the throughput reached.

The main technical problem that was encountered during this project relates to the machine characteristics necessary to run a ray tracing model. Initially it was intended to make a simulator that would take full advantage of 3D cartography and add the various functionalities necessary to achieve the desired result, but as this approach became unworkable due to the required high computing power (such as a few dozen of GB available in RAM and a very good processor), a model based on METIS was the way forward in order to continue the work previously developed with this type of models.

Given the results presented in section 4, since the results comparing the simulated values and the real ones are quite similar, this work can contribute to the development of studies in the area. In the walk-tests it was verified that 4G coverage was never a problem to carry out the tests in 5G except in 2 situations in which the UE connected to stations that were not anchor of the 5G network. It was also found that the coverage of the 5G network ”stretched” to areas with 4G coverage from non-colocalized cells and, as such, using Beamforming and other techniques such as Massive MIMO, it is possible to increase the coverage area and, in ultimately improve the end-user experience. Moreover, the simulator can predict when the terminal has coverage and which beams serve each user, thus increasing the capacity available on the network.

It is important to note that, given the approach of the type of simulator used and the assumption of the correspondence of the beam concept in the simulator, although it is possible to predict the conditions of the serving network, the distribution of users across the various beams may be different in real life. This is mainly due to the fact that there is no access to all the supplier's information and because the supplier has some freedom in adjusting users to beams using proprietary algorithms.

Thus, this work can contribute to the the development of future applications but it is recommended to change the type of used model to a model that can make these predictions more accurately, reducing the error between, for example, the estimated and the actual speed values.

References

[1] Ericsson, "Ericsson Mobility Report — Special edition World Economic Forum," Ericsson, Tech. Rep., Jan 2019. [Online]. Available: https://www.ericsson.com/assets/local/mobility-report/documents/2019/ericsson-mobility-report-world-economic-forum.pdf

[2] B. Sanou, "Setting the Scene for 5G: Opportunities & Challenges," Telecommunication Development Bureau, International Telecommunication Union, Tech. Rep. 978-92-61-27591-4, 2018. [Online]. Available: https://www.itu.int/en/ITU-D/Documents/ITU_5G_REPORT-2018.pdf

[3] Huawei Technologies Co., Ltd., "5G Spectrum: Public Policy Position," Huawei Technologies Co., Ltd., Tech. Rep., 2017. [Online]. Available: http://www-file.huawei.com/-/media/CORPORATE/PDF/public-policy/public_policy_position_5g_spectrum.pdf

[4] Ericsson. 5G spectrum: strategies to maximize all bands. [Online]. Available: https://www.ericsson.com/en/networks/trending/hot-topics/5g-spectrum-strategies-to-maximize-all-bands

[5] P. Chatterjee, "Wireless MIMO Driving RF Challenges — DigiKey," Dec 2012. [Online]. Available: https://www.digikey.com/en/articles/techzone/2012/dec/wireless-mimo-driving-rf-challenges

[6] W. Hong, Z. H. Jiang, C. Yu, J. Zhou, P. Chen, Z. Yu, H. Zhang, B. Yang, X. Pang, M. Jiang, Y. Cheng, M. K. T. Al-Nuaimi, Y. Zhang, J. Chen, and S. He, "Multibeam Antenna Technologies for 5G Wireless Communications," *IEEE Transactions on Antennas and Propagation*, vol. 65, no. 12, pp. 6231–6249, Dec 2017.

[7] G. Liu, Y. Huang, F. Wang, J. Liu, and Q. Wang, "5G features from operation perspective and fundamental performance validation by field trial," *China Communications*, vol. 15, no. 11, pp. 33–50, Nov 2018.

[8] A. Fragoso, "Impact of massive mimo antennas on high capacity 5g-nr networks," Master's thesis, Instituto Superior Técnico, 2019.

[9] European Telecommunications Standards Institute, "5G; NR; User Equipment (UE) radio transmission and reception; Part 1: Range 1 Standalone," 3GPP, Tech. Rep. TS 38.101-1

version 15.2.0 Release 15, Jul 2018. [Online]. Available: https://www.etsi.org/deliver/etsi_ts/138100_138199/13810101/15.02.00_60/ts_13810101v150200p.pdf

[10] ——, "5G; NR; User Equipment (UE) radio transmission and reception; Part 2: Range 2 Standalone," 3GPP, Tech. Rep. TS 38.101-2 version 15.4.0 Release 15, Apr 2019. [Online]. Available: https://www.etsi.org/deliver/etsi_ts/138100_138199/13810102/15.04.00_60/ts_13810102v150400p.pdf

[11] Xiaomi. Mi 10 Specs. [Online]. Available: https://www.mi.com/global/mi-10/specs/

[12] S. Asif, *5G Mobile Communications: Concepts and Technologies*. CRC Press, 2018.

[13] A. Kukushkin, *Introduction to mobile network engineering : GSM, 3G-WCDMA, LTE and the road to 5G*, 1st ed. John Wiley & Sons, 2018.

[14] GSMA, "5G Spectrum — GSMA Public Policy Position," GSMA, Tech. Rep., Jul 2018. [Online]. Available: https://www.gsma.com/spectrum/wp-content/uploads/2018/11/5G-Spectrum-Positions.pdf

[15] W. Webb, *The 5G Myth: When Vision Decoupled from Reality*. Walter de Gruyter, 2018.

[16] Ericsson, "3GPP Spectrum bands — 3GPP Release 16," Ericsson, Tech. Rep., Jul 2019. [Online]. Available: https://www.ericsson.com/4a341b/assets/local/policy-makers-and-regulators/190731-3gpp-spectrum-bands.pdf

[17] Devaki Chandramouli and Rainer Liebhart and Juho Pirskanen, *5G for the Connected World*. John Wiley & Sons Ltd, 2019.

[18] E. Ali, M. Ismail, R. Nordin, and N. F. Abdulah, "Beamforming techniques for massive MIMO systems in 5G: overview, classification, and trends for future research," *Front. Inf. Technol. Electron. Eng.*, vol. 18, no. 6, pp. 753–772, 2017.

[19] M. Giordani, M. Polese, A. Roy, D. Castor, and M. Zorzi, "A tutorial on beam management for 3gpp nr at mmwave frequencies," *IEEE Communications Surveys Tutorials*, vol. 21, no. 1, pp. 173–196, 2019.

[20] D. Kurita; et al., "Outdoor Experiments on 5G Radio Access Using BS and UE Beamforming in 28-GHz Frequency Band," *2019 16th IEEE Annual Consumer Communications & Networking Conference (CCNC)*, pp. 1–6, 2019.

[21] M. Matalatala, M. Deruyck, E. Tanghe, L. Martens, and W. Joseph, "Simulations of beamforming performance and energy efficiency for 5G mm-wave cellular networks," *IEEE Wireless Communications and Networking Conference, WCNC*, vol. 2018-April, pp. 1–6, 2018.

[22] J. F. Monserrat and M. Fallgren, “Simulation guidelines, deliverable 6.1 v1,” *METIS Project, 3GPP, Tech. Rep. ICT-317669*, vol. 6, April 2013.